

A proteomics-based systems genetics approach reveals environment-specific loci modulating protein co-expression and drought-related traits in maize

Running title: Systems genetics of drought-related traits in maize

Mélanie Blein-Nicolas^{1*}, Sandra Sylvania Negro¹, Thierry Balliau¹, Claude Welcker², Llorenç Cabrera Bosquet², Stéphane Dimitri Nicolas¹, Alain Charcosset¹, Michel Zivy^{1*}

¹ GQE– Le Moulon, INRA, Univ. Paris-Sud, CNRS, AgroParisTech, Université Paris-Saclay,

91190, Gif-sur-Yvette, France

² LEPSE, INRA, Univ Montpellier, SupAgro, Montpellier, France

* Corresponding authors:

michel.zivy@inra.fr, +33-1-69-33-23-65

melisande.blein-nicolas@inra.fr, +33-1-69-15-68-06

Keywords: proteomics, GWAS, drought, Zea maïs, mass spectrometry, integrative biology

18 **ABSTRACT**

20 The evolution of maize yields under drought is of particular concern in the context of
climate change and human population growth. To better understand the mechanisms associated with
22 the genetic polymorphisms underlying the variations of traits related to drought tolerance, we used a
systems genetics approach integrating high-throughput phenotypic, proteomics and genomics data
24 acquired on 254 maize hybrids grown under two watering conditions. We show that water deficit,
even mild, induced a strong proteome remodeling and a reprogramming of the genetic control of the
26 abundance of many proteins. We identify close co-localizations between QTLs and pQTLs, thus
highlighting environment-specific pleiotropic loci associated to the co-expression of drought-
28 responsive proteins and to the variations of phenotypic traits. These findings bring several lines of
evidence supporting candidate genes at many loci and provide novel insight into the molecular
30 mechanisms of drought tolerance.

32

34 INTRODUCTION

36 Maize is the main crop worldwide (Shiferaw et al. 2011) in terms of production. Although it
exhibits a high water use efficiency thanks to its C4 metabolism, it is also highly sensitive to water
38 deficit. As an illustration, maize is twice as much affected by drought as wheat, with 39.3% and
20.6% respective yield reductions associated with 40% reduction of water (Daryanto et al. 2016).
40 Improving maize yield under drought has been an important goal of breeding programs for several
decades (Campos et al. 2004, 2006; Cooper et al. 2014). However, despite the overall genetic
42 progress obtained, increases in drought sensitivity have been reported in several regions (Lobell et
al. 2014; Zipper et al. 2016; Meng et al. 2016). In addition, severe drought stress episodes are
44 projected to become more frequent in the near future due to climate change (Harrison et al. 2014).
Therefore, the evolution of maize productivity under water deficit is of particular concern and large
46 efforts are still required to design varieties able to maintain high yields in drought conditions.

One lever to accelerate the genetic progress is to better understand the genetic and molecular
48 bases of drought tolerance. This highly complex trait is associated to a series of mechanisms
occurring at different spatial and temporal scales to (i) stabilize the plant water and carbon status,
50 (ii) control the side effects of water deficit including oxidative stress, mineral deficiencies and
reduced photosynthesis and (iii) maintain the plant yield (Chaves et al. 2003). At the physiological
52 level, short-term responses include stomata closure, osmotic and hydraulic conductance
adjustments, leaf growth inhibition and root growth promotion (Tardieu et al. 2018). At the
54 molecular level, complex signaling and regulatory events occur, involving several hormones, of
which abscisic acid (ABA) is a key player, and a broad range of transcription factors (Golldack et
56 al. 2014; Osakabe et al. 2014; Tripathi et al. 2014). Molecular responses also include the
accumulation of metabolites involved in osmotic adjustment, membrane and protein protection or
58 scavenging of reactive oxygen species and the expression of drought-responsive proteins like
dehydrins, late embryogenesis abundant (LEA) and heat shock proteins (HSP) (Valliyodan and

60 Nguyen 2006; Seki et al. 2007). All these responses depend on the drought scenario, the
phenological stage, the genetic potential and the surrounding environment (Tardieu et al. 2018).
62 Altogether, the multiplicity and versatility of the mechanisms coming into play explain the
difficulty to select for drought tolerance.

64 Breeding new drought-tolerant varieties would greatly benefit from a better understanding
of the genotype-phenotype relationship. Systems genetics is a recent approach allowing to gain
66 better insight into this relationship by deciphering the biological networks and molecular pathways
underlying complex traits and by understanding how they are regulated at the genetic and epigenetic
68 levels (Nadeau and Dudley 2011; Civelek and Lusis 2014; Feltus 2014; van der Sijde et al. 2014;
Markowitz and Boutros 2015). It consists in comparing the position of quantitative trait loci
70 (QTLs) underlying phenotypic traits variation to that of QTLs underlying the variation of upstream
molecular phenotypes such as transcript expressions (eQTLs) or protein abundances (pQTLs). Until
72 now, this approach has been mostly applied in human and animals (Johnson et al. 2015; Williams et
al. 2016; Moreno-Moral and Petretto 2016) and to a lesser extent in plants (Moreno-Moral and
74 Petretto 2016; Munkvold et al. 2013; Ogura and Busch 2016; Basnet et al. 2016; Christie et al.
2017; Mizrachi et al. 2017).

76 The first studies that compared QTLs and pQTLs used 2D gel proteomics to quantify
proteins (Bourgeois et al. 2011; de Vienne et al. 1999). Since then, proteome coverage and data
78 reliability have been widely improved by the use of mass spectrometry (MS)-based proteomics
(Wasinger et al. 2013). Despite these progress, the systems genetics studies published so far have
80 preferentially used transcripts rather than proteins as intermediate level between the genome and
end-point phenotypes. One reason is that large-scale proteomics experiments remain challenging
82 (Blein-Nicolas et al. 2015) due to technical constraints (Balliau et al. 2018) and to the trade-off
between depth of coverage and sample throughput (Keshishian et al. 2017). Yet, proteins are
84 particularly relevant molecular components to link genotype to phenotype. Due to the buffering of

transcriptional variations and to the role of post-translational regulations in phenotypes

86 construction, proteins are indeed expected to be more highly related to end-point phenotypes than
transcripts (Foss et al. 2011; Battle et al. 2015; Chick et al. 2016; Albertin et al. 2013; Vogel and
88 Marcotte 2012).

Here, we aimed to better understand the molecular mechanisms associated with the genetic
90 polymorphisms underlying the variations of traits related to drought tolerance. To this end, we
performed a unique systems genetics study where MS-based proteomics data acquired for 254
92 maize genotypes grown in two watering conditions were integrated with high-throughput genomic
and phenotypic data. Protein abundances were first analyzed by using genome wide association
94 study (GWAS) and co-expression networks. Then they were integrated with phenotypic data
measured for drought-related trait in the same conditions (Prado et al. 2018) through correlation
96 analysis and search for QTL/pQTL co-localizations. We showed that water deficit, even mild,
caused a deep proteome remodeling associated to changes in the genetic architecture of protein
98 abundances. Some of these changes could also affect drought-related traits, as indicated by
QTL/pQTL co-localizations. These were underlied by exciting candidate genes. In particular, we
100 identified two transcription factors likely involved in the condition-specific co-regulation of
drought-responsive proteins as well as in the genetic variations of several phenotypic traits. We also
102 highlighted many cases of QTL/pQTL co-localizations with a reduced number of underlying
candidate genes.

104 RESULTS

106 Mild water deficit has extensively remodeled the proteome

Using MS-based proteomics, we analyzed more than 1,000 leaf samples taken from 254
108 genotypes representing the genetic diversity within dent maize and grown in well-watered (WW)
and water deficit (WD) conditions. After data filtering, our peptide intensity dataset included 977
110 samples corresponding to 251 genotypes from which we reliably quantified 1,950 proteins. For 977
of them that exhibited too many missing peptide intensity values, quantification was performed
112 based on the number of chromatographic peaks (PC-based set). For the remaining 973 proteins that
were on average more abundant (Sup. Figure 1A), quantification was performed based on peptide
114 intensities, that provide a higher precision of quantification than counting data (Sup. Figure 1B,
XIC-based set). Functional categories involving highly abundant proteins, such as energy
116 metabolism, were better represented in the XIC-based than in the PC-based set (Sup. Figure 1C).

Heatmap representations of protein abundances show that the two watering conditions were
118 well separated by two large protein clusters (Figure 1A), indicating that, although moderate, water
deficit has extensively remodeled the proteome of most genotypes. Accordingly, 82.4% and 71.7%
120 of the proteins of the XIC-based and PC-based sets respectively responded significantly to water
deficit (adjusted *P-value* < 0.05, WD/WW ratio > 1.5 or < 0.66, Sup. Table 1). These included
122 several proteins known to be involved in responses to drought or stress (hereafter named drought-
responsive proteins) such as dehydrins (GRMZM2G079440, GRMZM2G373522), ABA-responsive
124 protein (GRMZM2G106622), LEA protein (GRMZM2G352415), HSPs (GRMZM2G360681,
GRMZM2G080724, GRMZM2G112165), phospholipase D (GRMZM2G061969), glyoxalase I
126 (GRMZM2G181192) or glutathione-S-transferase (GRMZM2G043291). Induced and repressed
proteins constituted two populations highly differentiated in terms of function (Figure 1B). In
128 particular, transcription, translation, energy metabolism and metabolism of cofactors and vitamins

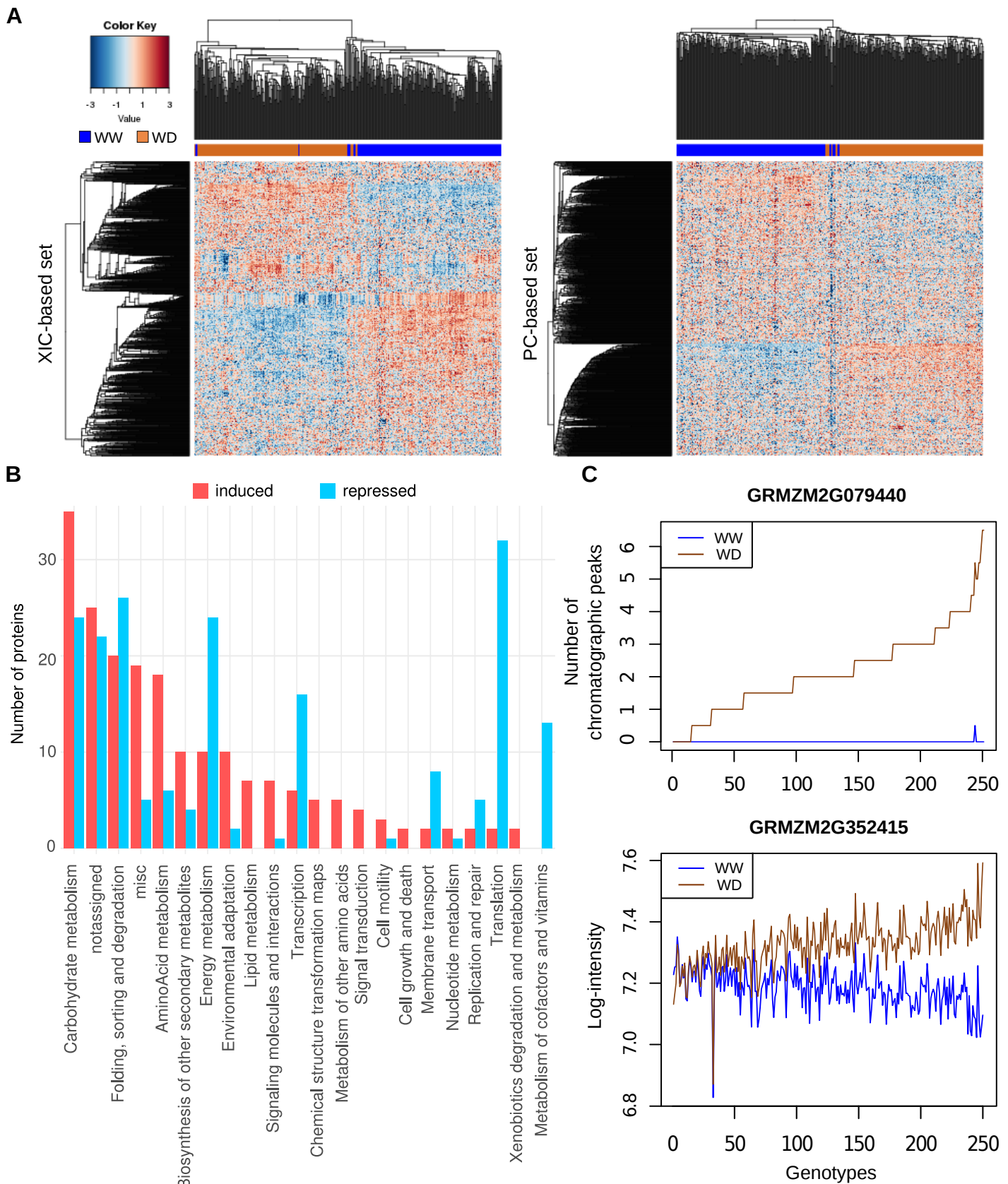


Figure 1. Effect of a mild water deficit on the proteome. (A) Heatmap representations of the abundances estimated for the XIC-based protein set (left) and the PC-based protein set (right). Each line corresponds to a protein and each column to a genotype x watering condition combination. For each protein, abundance values were scaled and represented by a color code as indicated by the color-key bar. Hierarchical clusterings of the genotype x watering condition combinations (top) and of the proteins (left) were built by using the 1-Pearson correlation coefficient as distance and the unweighted pair group method with arithmetic mean (UPGMA) as aggregation method. (B) Functions of the 200 most induced and 200 most repressed proteins under water deficit. (C) Abundance profiles of the RAB17 dehydrin (GRMZM2G079440 quantified based on the number of chromatographic peaks) and of a LEA protein (GRMZM2G352415 quantified based on peptide intensities) in the two watering conditions. Genotypes on the x axis were ordered according to the WD/WW abundance ratio.

were better represented within repressed proteins, while carbohydrate and amino acid metabolisms,
130 environmental adaptation, signaling molecules and interaction were better represented within
induced proteins.

132 The global impact of a genotypic change on the proteome was less extensive than that of
water deficit, since the proteomes of two different genotypes grown in the same watering condition
134 were more similar than the proteome of a same genotype grown in different conditions (Figure 1A).
However, the maximum amplitudes of abundance variations were similar (Sup. Figure 2). In
136 addition, 94.9% of the proteins from the XIC-based set exhibited significant genetic variations of
abundance (adjusted *P-value* < 0.05, fold change > 1.5 or < 0.66). This was confirmed by broad
138 sense heritability, the median of which was 0.47 and 0.46 for the WW and WD conditions,
respectively (Sup. Figure 3A). By contrast, in the PC-based set, only 37.4% of the proteins showed
140 significant genetic variations of abundance and the median of broad sense heritability was 0.07 and
0.09 in the WW and WD conditions, respectively (Sup. Figure 3B).

142 Regarding the genotype x environment (GxE) interactions, several results indicate that they
were larger in the PC-based than in the XIC-based set. The correlations of protein abundances
144 between the two watering conditions were lower in the former than in the latter (median of $r = 0.08$
and 0.44, respectively; Sup. Figure 4A). Furthermore, the contribution of the GxE interactions to
146 the total variability of protein abundances was higher in the PC-based than in the XIC-based set
(Sup. Figure 4B-D). However, significant GxE interactions were detected for only four and 15
148 proteins of the PC-based and XIC-based sets, respectively, probably because of a lack of statistical
power. These proteins included a LEA protein (GRMZM2G352415) and the ZmRab17 dehydrin
150 (GRMZM2G079440), the latter being undetectable in the WW condition and more or less expressed
depending on the genotype in the WD condition (Figure 1C).

152

154 **Genetic architecture of protein abundance is related to protein function**

To identify pQTLs, we submitted the 3,900 molecular phenotypes (1,950 proteins x 2
156 watering conditions) obtained from the proteomics analysis to GWAS. In total, we detected 583,288
(163,674 in the PC-based set and 419,614 in the XIC-based set) significant associations (P -value <
158 10^{-5}) for 3,759 (96.4%) molecular phenotypes. Associated SNPs explained between 0.3 and 83.2%
of variance, with an average at 8.7% (Sup. Figure 5).

160 To summarize associated SNPs into pQTLs, we developed a geometric method based on the
 P -value signal of SNPs. Compared to classical methods based on the genetic distance or on linkage
162 disequilibrium (LD), it allowed to detect the lowest number of pQTLs per molecular phenotype
(median at 8, 10 and 7, respectively) and the lowest maximum number of pQTLs per chromosome
164 (57, 209 and 15, respectively). It also produced the lowest correlation between the number of
pQTLs per chromosome and the P -value of the most strongly associated pQTL on the
166 corresponding chromosome (Sup. Figure 6). In total, we thus detected 29,004 pQTLs (16,911 and
12,093 in the XIC-based and PC-based sets, respectively; sup. Table 2). The median number of
168 pQTLs per molecular phenotype was 8 and 5 for the XIC-based and PC-based sets, respectively
(Sup. Figure 7A). 1,385 (4.8%) pQTLs were local, *i.e.* located at less than 10^6 bp from the protein
170 encoding gene, of which 442 were located within the genes. Among the distant pQTLs, 81.7% were
located on a chromosome different than that of the protein encoding gene. Local pQTLs had
172 stronger effects than distant pQTLs (average $R^2=19.3\%$ and 5.5% , respectively; Sup. Figure 7B).
For 992 proteins, no local pQTL was detected in any of the conditions. Compared to the 816
174 proteins showing a local pQTL in at least one condition, these proteins were significantly enriched
in proteins involved in translation (13.6% vs 4.2% , adjusted P -value = $4.8e^{-11}$) and energy
176 metabolism (11.2% vs 6.9% , adjusted P -value = 0.016) and depleted in proteins involved in
carbohydrate metabolism (10.5% vs 18.1% , adjusted P -value = $4.2e^{-05}$). They also exhibited less
178 distant pQTLs (Sup. Figure 8 A, B) and were much less heritable (Sup Figure 8 C, D). These results

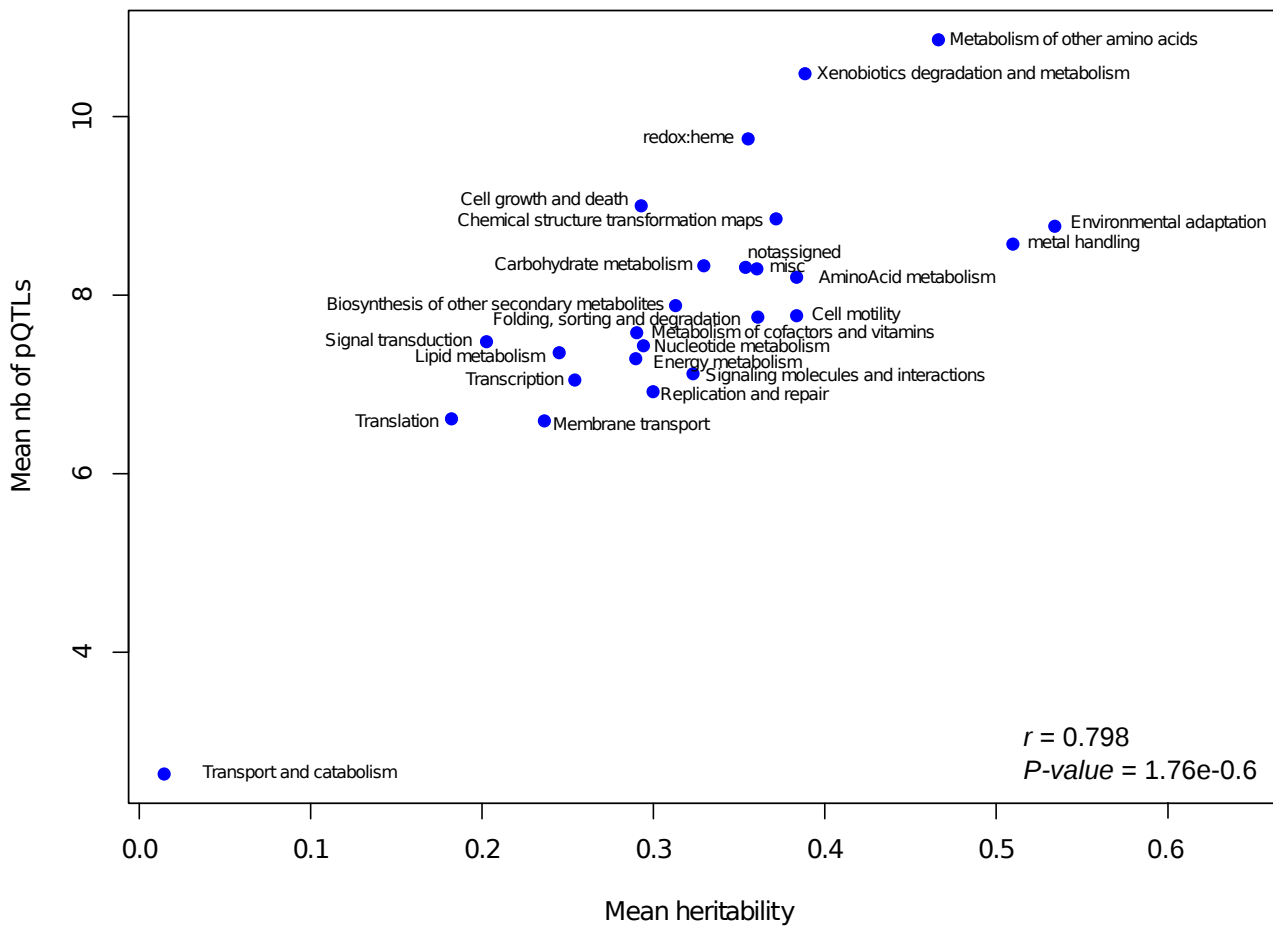


Figure 2. Relationship between the mean number of pQTLs per KEGG category and the mean heritability per KEGG category.

indicate that genetic regulation of protein abundances depends on protein function. This observation
180 is supported by the positive correlation between the mean number of pQTLs and the mean
heritability per functional category (Figure 2).

182

Identification of genomic regions with pleiotropic effects on the proteome

184 pQTLs were not uniformly distributed in the genome (Figure 3). Instead, there were
genomic regions enriched with pQTLs. We detected 25 and 23 of such hotspots that contained more
186 than 20 pQTLs in the WW and WD conditions, respectively (Sup. Table 3). For 15 and 13 of them
respectively, the abundances of the associated proteins were more strongly correlated than expected
188 by chance (P -value < 0.01; sup. Figure 9, Sup. Table 3), which indicates an enrichment in co-
expressed proteins. These hotspots might thus represent regulatory loci with pleiotropic effects on
190 the proteome.

To complement these results, we performed a weighted gene co-expression network analysis
192 (WGCNA) of protein co-expression across the 251 genotypes in the two watering conditions
separately. Co-expression networks in the WW and WD conditions captured 1,671 proteins in 11
194 modules and 1,578 proteins in 14 modules, respectively (Figure 4, Sup. Table 4). Each module
contained 31 to 377 proteins. The WD network was well structured according to protein function
196 with many modules showing significant functional enrichments (Figure 4, Sup. Table 5). Because
most modules were well preserved between conditions (Sup. Figure 10A, B), we could build a
198 consensus network capturing 698 proteins and composed of 15 modules containing 14 to 197
proteins (Figure 4, Sup. Figure 10C; Sup. Table 4). Consensus modules were more particularly
200 enriched in photosynthesis proteins, ribosomal proteins and in proteins involved in mitochondrial
electron transport, ATP synthesis and in the tetrapyrrole pathway (Figure 4, Sup. Table 5). Two
202 modules were condition-specific (Figure 4, Sup. Figure 10). Note that the module specific of the
WD condition and was significantly enriched for drought-responsive proteins (Sup. Table 5).

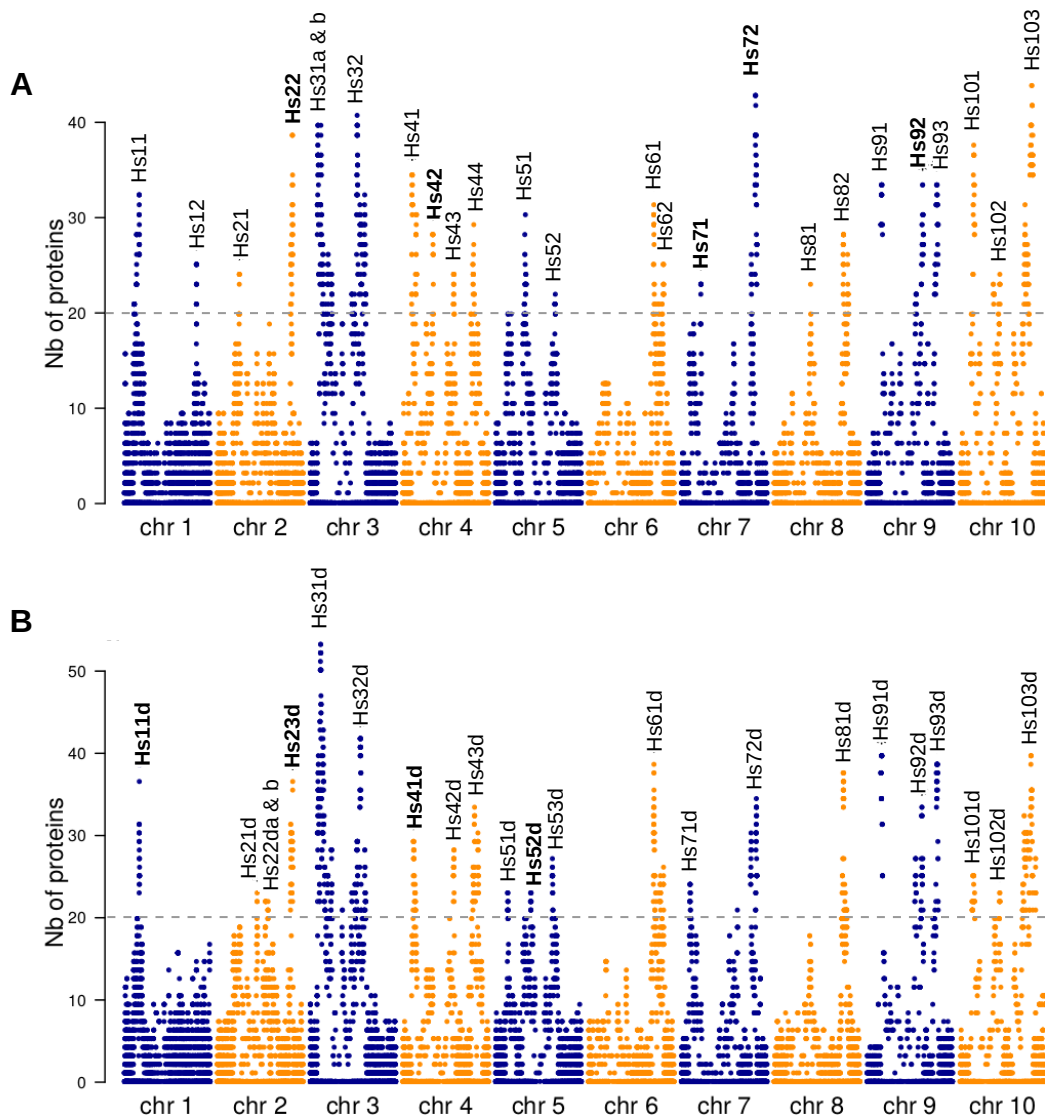


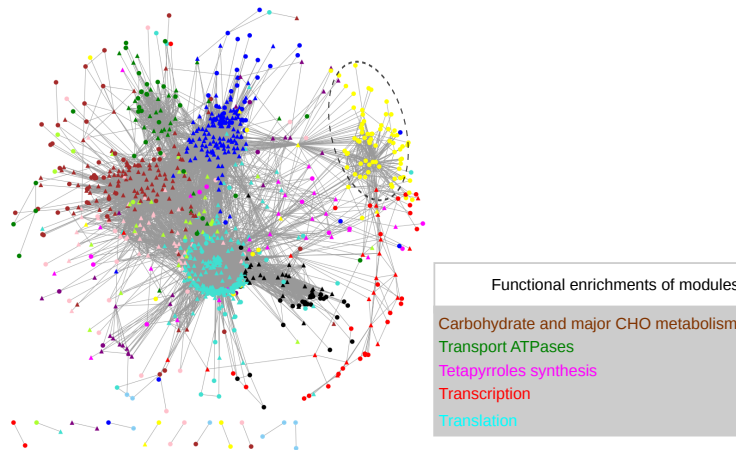
Figure 3. Distribution of pQTLs along the genome. (A) In the well-watered condition. (B) In the water deficit condition. Each point indicates the number of proteins controlled by a pQTL located in a given genomic region defined by the linkage disequilibrium interval around a SNP. Dashed horizontal lines indicate the arbitrary threshold used to detect pQTL hotspots. Names and positions of the pQTL hotspots are indicated above each graph. Names in bold indicate pQTL hotspots confidently detected as potential pleiotropic loci (see Sup. Table 3 for details).

204 Protein abundances within each module were summarized into variables called eigengenes
that were considered as molecular phenotypes and submitted to GWAS. In total, we detected 2,859
206 significant associations ($-\log_{10}(P\text{-value}) > 5$) for 55 eigengenes (11, 14 and 30 for WW, WD and
consensus modules, respectively). Significantly associated SNPs were summarized into 369 co-
208 expression QTLs (coQTLs, Sup. Table 2). When a coQTL co-localized with a pQTL hotspot, we
checked whether the proteins associated to the hotspot were significantly enriched for proteins
210 belonging to the module controlled by the coQTL ($P\text{-value} < 0.01$). Thus crossing the results, we
confirmed nine hotspots as potential pleiotropic loci. Five of them were in the WW condition
212 (Hs22, Hs42, Hs71, Hs72 and Hs92) and four were in the WD condition (Hs11d, Hs23d, Hs41d and
Hs52d; Sup. Table 3). Remarkably, several of these hotspots were associated to proteins exhibiting
214 consistent functions. For example, hotspots Hs42 and Hs23d were mainly associated to ribosomal
proteins (Sup. Table 6) and hotspots Hs71 and Hs72 were associated to proteins involved in energy
216 metabolism and more particularly ATP synthesis and photosynthesis.

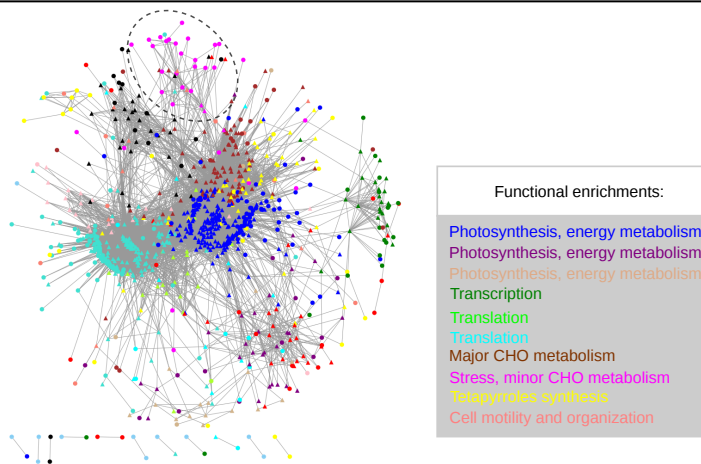
218 **The genetic architecture of protein abundances depends on the environment**

Of the 14,432 pQTLs detected in the WW condition, only 1,212 (8.4%) had a co-localizing
220 pQTL in the WD condition. These pQTLs were generally of strong effects (Sup. Figure 11A) and
were enriched for local pQTLs (37.7% vs 4.8% in the whole dataset). Interestingly, while most of
222 the pQTLs shared across conditions had similar effects in the two conditions, 80 of them (6.6%)
exhibited contrasted effects (Sup. Figure 11B). Half of these pQTLs were local, suggesting that
224 gene promoters may be involved in the GxE interaction or that the pQTLs detected in each
condition corresponded to different polymorphic sequences with different effects on protein
226 abundances. These pQTLs were associated to 75 proteins, several of which were drought-
responsive (Sup. Table 7).

WW network



WD network



Consensus network

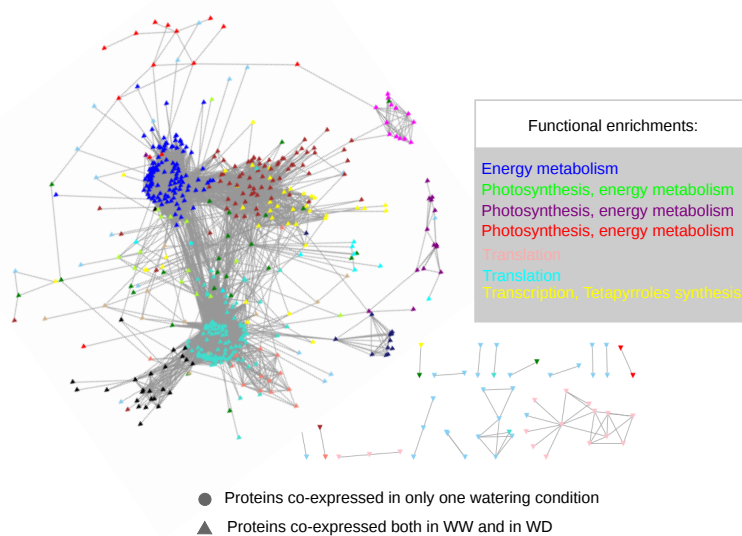


Figure 4. Graphical representation of the co-expression networks resulting from the WGCNA analyses. Only proteins showing adjacencies > 0.02 are shown. The consensus network contains the proteins that were co-expressed in the two watering conditions. The three views were created by Cytoscape v3.5.1 using an unweighted, spring-embedded layout. The colors displayed on each network represent the different modules identified by WGCNA. Functional enrichments of modules are indicated in grey boxes. Condition-specific modules are surrounded by dashed circles.

228 As observed for individual proteins, eigengenes for consensus modules were poorly to
moderately correlated between conditions (r between -0.03 to 0.62, Sup. Figure 12) and only one
230 coQTL was shared across conditions. Regarding the nine cross-validated pQTL hotspots, one co-
localization was found between Hs22 and Hs23d. However, these two hotspots shared only one
232 associated protein, suggesting that they represented two different loci. Altogether, these results
indicate that the positions of genomic regions with pleiotropic effects on the proteome also
234 depended on the environment.

236 **Identification of genomic regions involved in multi-scale genetic control**

To gain insight into the molecular mechanisms associated to drought tolerance, we searched
238 for co-localizations between the pQTLs, coQTLs or hotspots detected in our study and the 160
QTLs detected by Alvarez Prado *et al.* (2018) on the same plant material. These QTLs controlled
240 eight phenotypic traits related to growth and transpiration rate in the WW and WW conditions: leaf
area early (*i.e.* before water deficit; LAe), leaf area late (LAl), biomass early (Be), biomass late
242 (Bl), water use (WU), water use efficiency (WUE), stomatal conductance (gs) and transpiration rate
(Trate). To select for robust co-localizations, we took into account the correlations corrected by the
244 structure and kinship between the trait values and the protein abundances or the module eigengenes
($|r_{corrected}| > 0.3$).

246 In total, we identified 59 pairs of SNPs corresponding to QTL/pQTL co-localizations
(Figure 5, Sup. Table 8). They involved six phenotypic traits (Bl, LAl, WU, WUE, Trate and gs) and
248 42 proteins, many of which were drought-responsive (Table 1). Most QTL/pQTL co-localizations
(96.6%) were detected in the WD condition, where they corresponded to 40 of the 91 QTLs
250 reported in this condition (Prado et al. 2018). All but one involved distant pQTLs. For 12 cases out
of 59 (20%), the co-localizing QTL and pQTL were represented by the same SNP. In most of the
252 remaining cases, the QTL/pQTL distance was less than 100 Kb (Figure 6A). Seventeen proteins

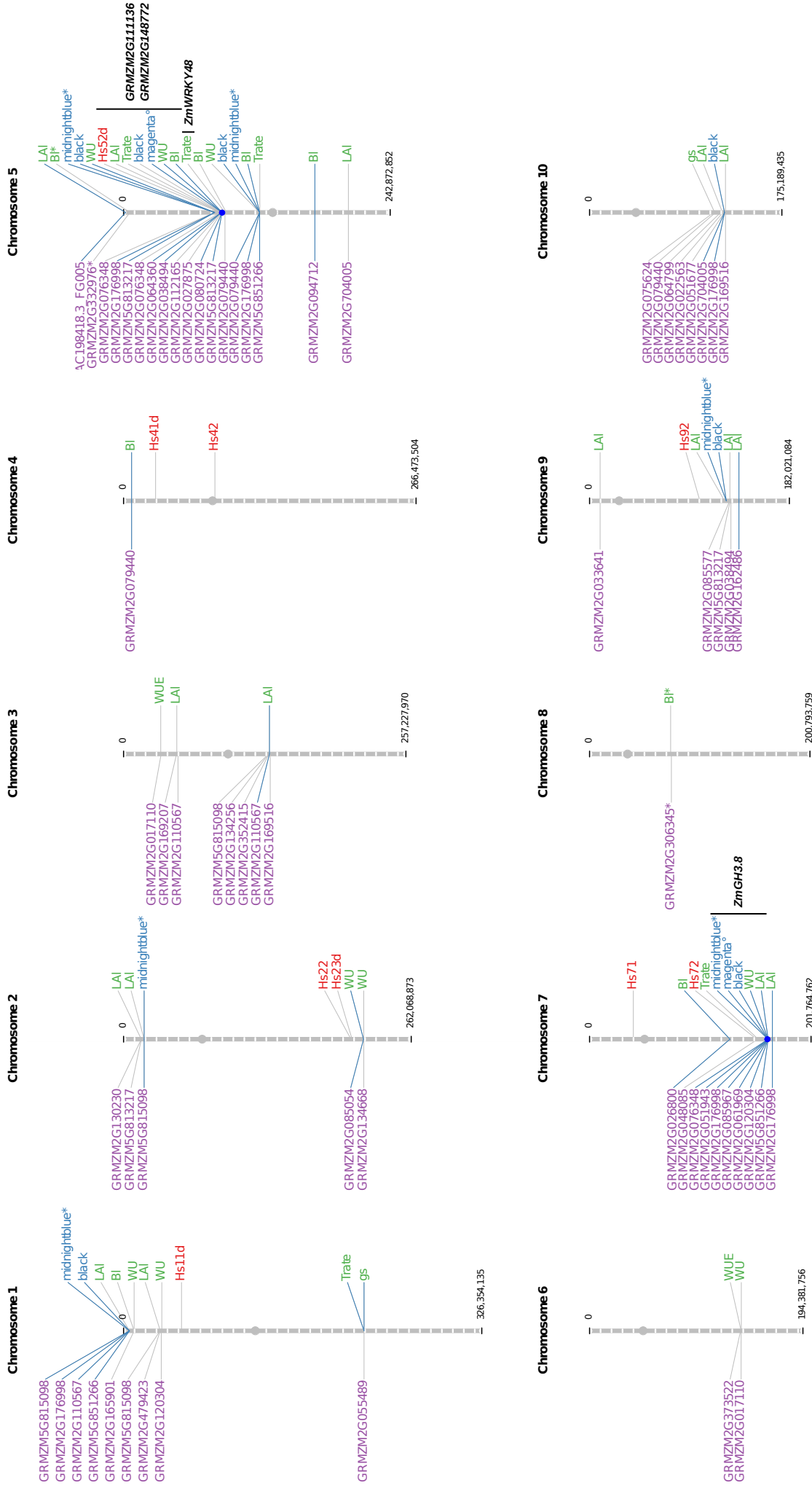


Figure 5. Genomic positions of the co-localizing pQTLs, coQTLs and QTLs. The positions of the nine pQTL hotspots robustly identified as potential loci with pleiotropic effects are indicated as well as the position of the most promising candidate genes. Chromosomes are segmented in 1 Mb bins. Grey dots represent the centromeres and blue dots indicate the position of genomic regions showing evidences for pleiotropy both at the proteome and phenotype level. Blue lines indicate pQTLs, coQTLs and QTLs that are determined by a same SNP. * consensus module, ° WD-specific module

exhibited multiple QTL/pQTL co-localizations (eight at maximum, Table 1). In particular, the
254 ZmRab17 protein presented seven QTL/pQTLs co-localizations involving four traits (Bl, Trate, WU
and gs with respectively 3, 2, 1 and 1 co-localizations; Sup. Table 8). LAI was the trait that
256 exhibited the highest number of co-localizations (44) involving 29 proteins and 16 QTLs (Sup.
Table 8).

258 We further identified 13 pairs of SNPs corresponding to QTL/coQTL co-localizations, all in
the WD condition (Sup. Table 9). They involved four phenotypic traits (WU, Bl, LAI and Trate) and
260 three modules including the WD-specific module (Figure 5). Eleven of the 13 QTLs co-localizing
with coQTLs also co-localized with pQTLs. The remaining two QTLs (at SNPs S5-88791868 on
262 chromosome 5 for Trate and AX-91801223 on chromosome 9 for LAI) actually also co-localized
with pQTLs, but with low correlations between the trait values and the protein abundances ($|r_{corrected}|$
264 < 0.06 ; Sup. Table 9). By contrast, the correlations between the trait values and the module
eigengenes were much higher ($|r_{corrected}| = 0.32$ and 0.50 , Sup. Table 9).

266 Taken together, these results indicate the presence of genomic regions involved in the
genetic control of traits at different levels of biological complexity. Some of these regions may
268 control multiple proteins which are more strongly related to end-point phenotypes when taken
collectively through co-expression module rather than individually. These results also revealed two
270 genomic regions showing evidences for pleiotropy both at the proteome and phenotype levels
(Figure 5). The first, located on chromosome 5 and spanning 1,8 Mb between SNPs AX-91657926
272 and AX-90612012, contained pQTLs for seven proteins, coQTLs for two modules and QTLs for
four phenotypic traits (LAI, BL, WU, and Trate). This region was also covered by hotspot Hs52d.
274 The second is on chromosome 7 where a single SNP (S7_162671160) determined the positions of
pQTLs for seven proteins, coQTLs for three modules and QTLs for two phenotypic traits (LAI and
276 WU).

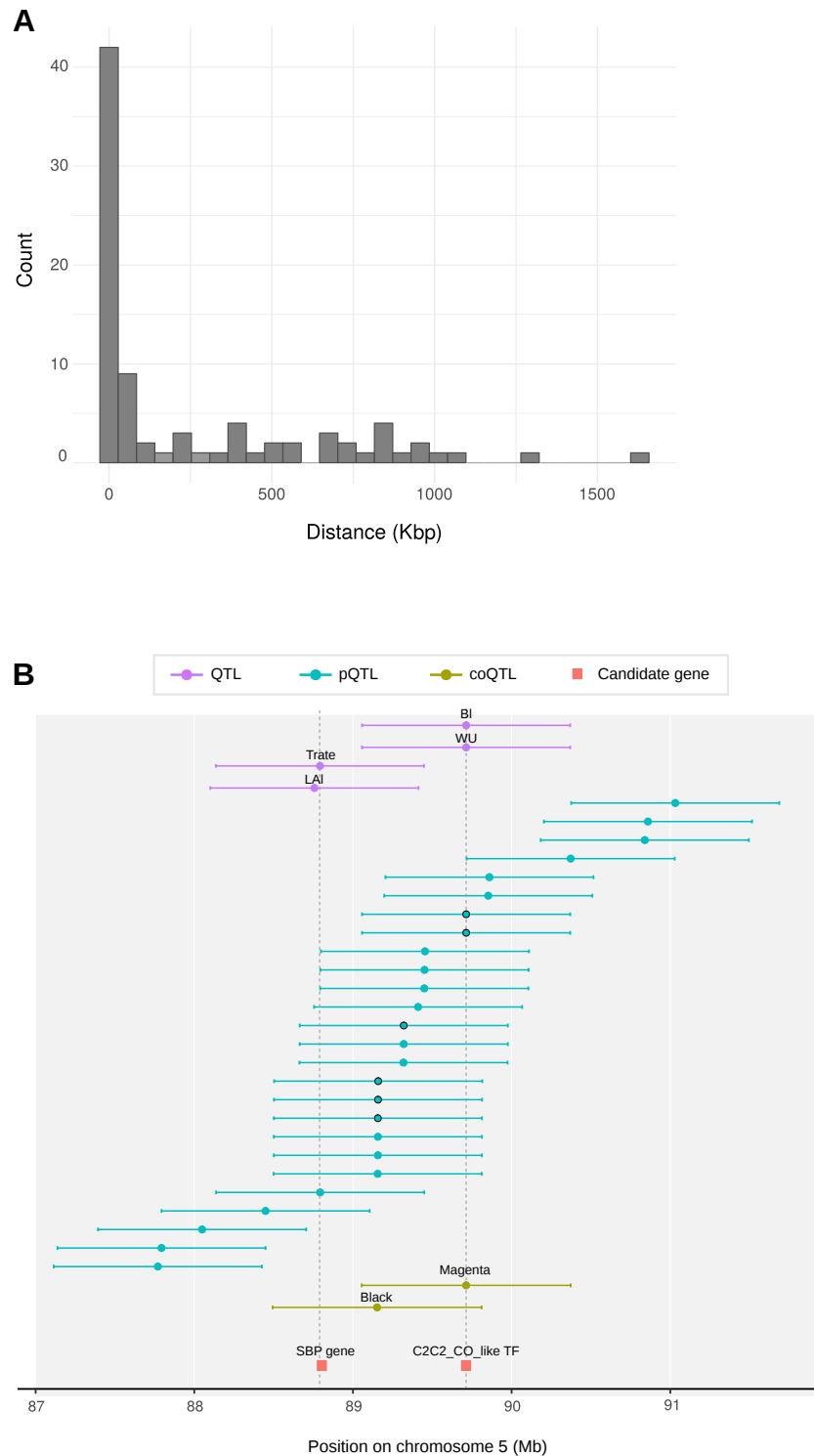


Figure 6. Identification of genomic regions involved in multi-scale genetic control.

(A) Distribution of the distances between co-localizing QTLs and pQTLs. (B) Detailed view of the QTL, pQTL, coQTL detected in the region covered by the hotspot Hs52d on chromosome 5. Dots represent the SNPs determining the position of the QTLs and horizontal bars represent the linkage disequilibrium-based window around each SNP. Black circled dots indicate the pQTLs that co-localize with QTLs or coQTLs with high correlations between the protein abundance and the phenotypic trait value or the module eigengene. Vertical dashed lines indicate the position of SNPs S5_88793314 (on the left) and AX-91658235 (on the right). The position of two transcription factors (a SBP gene, GRMZM2G111136, and a C2C2-CO-like transcription factor, GRMZM2G148772) representing promising candidate genes are indicated.

278 **Unraveling the molecular mechanisms associated to genetic factors underlying the variations** **of traits related to drought tolerance**

280 Assuming that the genetic determinants controlling the variations of both phenotypic traits
and protein abundances (or module eigengenes) were genes, we retrieved the genes underlying the
282 QTL/pQTL (or QTL/coQTL) co-localizations. We thus obtained a list containing one to 45
candidate genes for each of the 64 pairs of SNPs corresponding to QTL/pQTL or QTL/coQTL co-
284 localizations (Sup. Table 10). Based on gene annotation and literature, we identified in most cases
interesting candidate genes involved in hormone metabolism, regulation of transcription, signaling,
286 stress or drought response. Three cases especially caught our attention.

First, on chromosome 7, the SNP S7_162671160, mentioned above for its pleiotropy, was
288 located in the *ZmGH3.8* gene (GRMZM2G053338 encoding an auxin-response factor). In
agreement with the role of *ZmGH3.8* in drought response (Feng et al. 2015), S7_162671160 was
290 associated to the WD-specific module and to five stress proteins (endochitinase
GRMZM2G051943, beta-D-glucanase GRMZM2G073079, peroxidase GRMZM2G085967,
292 polyphenol oxydase GRMZM5G851266 and phospholipase D GRMZM2G061969). These results
indicates that *ZmGH3.8* may be the regulator underlying the QTLs, pQTLs and coQTLs located at
294 SNP S7_162671160.

Second, on chromosome 5, we identified a QTL for Trate which co-localized with a pQTL
296 associated to the *ZmRab17* dehydrin in the WD condition. Among the six genes underlying both the
QTL and the pQTL is the transcription factor *ZmWRKY48* (GRMZM2G120320), which has been
298 shown to be induced by water deficit (Song et al. 2017). This gene is orthologous to *AtWRKY40*,
which can bind to a W-box sequence in the promoter of the *AtRab18* gene and repress its expression
300 (Shang et al. 2010). *ZmRab17* is orthologous to *AtRab18* and also contains a W-box sequence in a
region upstream of the 3'UTR. Altogether, these results indicate that *ZmWRKY48* probably controls
302 the abundance of *ZmRab17*.

Third, in the region of chromosome 5 covered by hotspot Hs52d (Figure 5), there were 14
304 candidate genes, of which two can potentially control a high number of genes. One is a squamosa
promoter-binding (SBP) gene (GRMZM2G111136) shown to be induced by various abiotic stresses
306 including drought (Mao et al. 2016). The other, a C2C2-CO-like transcription factor
(GRMZM2G148772), was shown to be significantly induced by drought and salinity stress in B73
308 leaves (Forestan et al. 2016). Hotspot Hs52d covered a region of ca 4 Mb in which we detected 26
pQTLs, many of which were located between the SBP gene and the C2C2-CO-like transcription
310 factor (Figure 6B). In this region, there were also coQTLs for two modules and QTLs for WU, Bl,
Trate and LAI. Interestingly, a single SNP, AX-91658235 located only one kbp from the C2C2-CO-
312 like transcription factor, determined the position of two QTLs, two pQTLs and one coQTL.
Furthermore, SNP S5_88793314, that fell into the coding sequence of the SBP gene, determined the
314 position of a QTL for Trate and of a pQTL. Based on these results, we can hypothesize that hotspot
Hs52d may in fact correspond to two trans-acting regulators for which the SBP gene and the C2C2-
316 CO-like transcription factor represent good candidates.

318

DISCUSSION

320

In order to better understand the molecular mechanisms associated with the genetic
322 polymorphisms underlying the variations of traits related to drought tolerance, we analyzed the
proteomes of 254 dent maize genotypes grown in two watering conditions. By combining two
324 complementary MS-based quantification methods (XIC and PC-based), we reliably quantified
nearly 2,000 proteins in an unprecedented number of samples (>1,000). To our knowledge, this is
326 the best compromise ever obtained in MS-based proteomics between the number of samples
analyzed and the number of proteins quantified. Compared to the PC-based set, the proteins of the
328 XIC-based set exhibited higher heritabilities and more genetic variations of their abundances. These
discrepancies probably partly arose from the difference of precision in protein quantification.

330 Based on high-density genotyping data, we subsequently performed GWAS for ca. 4,000
molecular phenotypes, thus mapping 29,004 pQTLs at high-resolution. To achieve this result, we
332 had to summarize associated SNPs into pQTLs. This issue emerged only recently with the advent of
high marker densities and no gold standard method is currently available. Here, we developed a
334 geometric method based on the *P-value* signal of SNPs which allowed to take into account that the
number of significantly associated SNPs increased with the association strength. To our knowledge,
336 this relationship has never been reported before. We did not go further on this issue which was
outside the scope of this study. Nonetheless, our work opens the way towards new methodological
338 developments accounting for the strength of SNP associations for the detection of pQTLs.

Local pQTLs explained a higher proportion of the variance of protein abundance than
340 distant pQTL. They also revealed that the genetic architecture of protein abundances is related to
protein function. Notably, proteins involved in translation and in energy synthesis exhibited few
342 associated pQTLs with a lack of local pQTLs. These two functional categories were also
particularly well represented in consensus modules, in agreement with previous results showing that

344 genes in consensus modules had few associated eQTLs (Munkvold et al. 2013). As translation and
energy metabolism mainly contain ancient and evolutionarily conserved proteins (Goldman et al.
346 2010; Nelson and Junge 2015), our results suggest that the expression of evolutionarily ancient
proteins is more constrained with fewer associated pQTLs (Mähler et al. 2017; Popadin et al. 2014;
348 Zhang and Yang 2015). They also support the recent hypothesis of Mähler *et al.* (2017) that, for
genes experiencing reduced rates of molecular evolution, purifying selection on individual SNPs is
350 associated to stabilizing selection on gene expression.

pQTLs were distributed throughout the genome but some of them clustered into hotspots,
352 suggesting the presence of regulatory loci with large pleiotropic effects on the proteome. The
detection of such hotspots is highly dependent on the mapping resolution and on the method used to
354 cluster eQTLs or pQTLs, which may explain the contrasted results reported in the literature. Indeed,
while several studies report hotspots associated to hundreds of transcripts (Munkvold et al. 2013;
356 Christie et al. 2017; Orozco et al. 2012), others detected hotspots associated to only a few tens of
transcripts or proteins (Foss et al. 2011; Ghazalpour et al. 2011; Albert et al. 2014) or even no
358 hotspot at all (Mähler et al. 2017). In our study, false hotspot detection was limited by the high
mapping resolution and by the use of a pQTL clustering method taking into account the variations
360 of LD across the genome (Negro *et al.*, in print). Despite this, we cross-validated only five hotspots
in WW and four in WD based on protein co-expression and co-localization with coQTLs. The
362 positions of these hotspots were not shared across conditions. These results indicate that
polymorphic loci responsible for the variations in abundance of tens or hundreds of proteins are
364 scarce and can interact with the environment.

By analyzing a diversity panel of 254 genotypes, we showed that many small abundance
366 changes, detected as significant because they occurred in a high number of genotypes, contributed
to extensively remodel the proteome under water deficit. In total, approximately 75% of the
368 quantified proteins responded significantly to the environmental change. Up- and down regulated

proteins were well differentiated in terms of function and indicate that the photosynthetic,
370 transcriptional and translational machineries were slowed down while stress response and
signalization mechanisms were activated. All these changes show that plants clearly perceived a
372 lack of water and presented a coordinated proteome response to the environmental change.

Interestingly, the abundance changes occurring in response to water deficit were not
374 associated with major changes in the structure of the co-expression network since most co-
expression modules were more or less preserved in both conditions. Nonetheless, we identified a
376 WD-specific module that was significantly enriched for drought-responsive proteins. Similarly,
Munkvold *et al.* (2013) observed condition-specific modules related to biological processes
378 responsive to particular environmental conditions. Such modules suggest that, under environmental
perturbation, sets of genes or proteins are collectively mobilized by condition-specific factors
380 allowing the plant to adapt. In agreement with this hypothesis, the WD-specific module was
associated to several QTL/coQTL colocalizations, with high correlations between its eigengene and
382 the phenotypic traits values. In the case of transpiration rate, this correlation was even better than
with any of the proteins in the module. This indicates that drought-responsive proteins are major
384 contributors to the phenotypes, an observation reinforced by the fact that many QTL/pQTL co-
localizations involved such proteins. Remarkably, one coQTL for the WD-specific module was
386 located in a region of chromosome 5 that also cumulated several QTLs, pQTLs and the hotspot
Hs52d. This indicates that the co-expression observed for drought-responsive proteins may be
388 driven by condition-specific factors, the pleiotropic effects of which resonate across all layers of
biological complexity up to end-point phenotypes.

390 Linking phenotypic to proteome variations revealed many QTL/pQTL co-localizations for
which, thanks to the high mapping resolution, we identified a restrained number of candidate genes.
392 Among these, it is noteworthy to mention *ZmWRKY48* underlying a QTL for transpiration rate and
a pQTL for the *ZmRab17* protein that is specifically expressed under water deficit. *ZmWRKY48* is a

394 transcription factor known to be induced by water deficit in maize (Song et al. 2017) and its role in
the abundance variations of *ZmRab17* is strongly supported by the literature data available on
396 *AtWRKY40* and *AtRAB18* in *Arabidopsis* (Shang et al. 2010).

Surprisingly, only two of the 69 QTLs detected in the WW condition were involved in pQTL
398 co-localizations, while in the WD condition, 40 of the 91 QTLs co-localized with at least one
pQTL. To explain this discrepancy, we assume that under non-stress condition, phenotypic
400 variations were driven by many low contribution proteins probably controlled by low effect pQTLs
while under water stress, phenotypic variations were mainly driven by drought-responsive proteins
402 under the genetic control of condition-specific regulators. In agreement with this hypothesis, we
robustly identified two genomic regions that may correspond to such regulators. The first is located
404 on chromosome 7, where we identified the auxin response factor (ARF) *ZmGH3.8* as the unique
candidate gene underlying QTLs for leaf area and water use, pQTLs for seven proteins of which
406 five were involved in stress responses and coQTLs for three co-expression modules including the
WD-specific module. ARFs play key roles in plant growth and development through the regulation
408 of expression of auxin response genes which can include transcription factors (Li et al. 2016). They
are also thought to contribute to drought tolerance (Feng et al. 2015; Zhang et al. 2017). In maize
410 shoots, Feng *et al.* (2015) indeed showed that the expression of *ZmGH3.8* was induced by auxin and
reduced under polyethylene glycol treatment. More recently, Zhang *et al.* (2017) identified 13 ARFs
412 as differentially expressed between a drought tolerant and a drought sensitive maize line under
different drought scenarios. The second region is located on chromosome 5 where we identified two
414 transcription factors, a SBP gene (GRMZM2G111136) and a C2C2-CO-like gene
(GRMZM2G148772), as candidate genes underlying QTLs for key plant growth and transpiration
416 traits, pQTLs for seven proteins and coQTLs for three modules. This region also contained the
pQTL hotspot Hs52d. Both GRMZM2G111136 and GRMZM2G148772 were previously shown to
418 be induced by drought in maize (Mao et al. 2016; Forestan et al. 2016). In addition, SBP genes

constitute a functionally diverse family of transcription factors involved in plant growth and
420 development (Preston and Hileman 2013). Due to their potential implication in the GxE interactions
as pleiotropic, condition-specific regulator and because of their roles in both plant growth and
422 development and in drought response, *ZmGH3.8*, the SBP gene and the C2C2-CO-like transcription
factor represent particularly promising candidates for drought tolerance breeding.

424 To conclude, by using a systems genetics approach including MS-based proteomics data, we
highlighted several original results. We showed that water deficit, even mild, strongly remodeled
426 the proteome and induced a reprogramming of the genetic control of the abundance of many
proteins and notably those involved in drought responses. Furthermore, we point out that the genetic
428 architecture of protein abundances is related to protein function and also probably to the
evolutionary constraints on protein expression. Finally, we found QTL/pQTL co-localizations
430 mostly in the WD condition and we identified exciting candidate genes in the vicinity of WD-
specific polymorphisms responsible for both the co-expression of drought-responsive proteins and
432 the variations of drought-related traits. This suggests that the reprogramming of the genetic control
observed at the proteome level may also affect end-point phenotypes. Taken together, our results
434 demonstrate that proteomics has now reached enough maturity to be fully exploited in systems
studies necessitating large-scale experiments. Our findings also provide novel insights into the
436 molecular mechanisms of drought tolerance and highlight some pathways for further research and
breeding.

438 **METHODS**

440 **Plant material and experiment**

A diversity panel of maize hybrids obtained by crossing a common flint parent (UH007) with 254 dent lines was used (Millet et al. 2016). The flint line was used as the paternal parent. The experiment was carried out as in Prado *et al.* (2018). Plant growth conditions (type of soil used, temperature, light, irrigation) are described in full details in the aforementioned publication. Briefly, plants were sown on May 14, 2012 and grown in pots in the phenotyping platform PhenoArch (Cabrera-Bosquet et al. 2016) (https://www6.montpellier.inra.fr/lepse_eng/M3P/PHENOARCH-platform) hosted at the Montpellier Plant Phenotyping Platforms (https://www6.montpellier.inra.fr/lepse_eng/M3P). Two levels of soil water content were applied: well-watered (WW, soil water potential of -0.05 MPa) and water deficit (WD, soil water potential of -0.45 MPa). Hybrids were replicated three times in each of the watering condition.

Sampling was performed at the pre-flowering stage (between June 19 and June 22, 2012) in two replicates per hybrid and water condition. For each sampled plant, 35 to 45 mg of fresh material was taken in a 2 mL tube containing two iron metal beads (5 mm diameter) by punching ten patches (5 mm diameter) in the mature area of the last ligulated leaf. The tubes were frozen in liquid nitrogen immediately after sampling and stored at -80°C until protein extraction.

456

Protein extraction and digestion

Leaf patches were turn into powder by shaking frozen sample tubes twice at 20 Hz for 20 seconds using TissueLyzer II (Quiagen, Courtaboeuf, France). Beads were removed using a magnet. Proteins were precipitated by incubating the leaf powder in 1.2 ml of an ice-cold solution of acetone containing 10% of trichloroacetic acid and 0.07% β -mercaptoethanol for 1h20 at -20°C. After centrifugation (10 min, 0°C, 14 000 rpm), the supernatants were removed and the protein extracts

were washed by incubation in 1.2 ml of 0.07% β -mercaptoethanol in acetone (1h, -20°C). This step
464 was repeated twice. After the last washing, proteins were dried in a vacuum centrifuge and stored at
-80°C until solubilization.

466 Dried protein pellets were solubilized in 100 μ l of a solution containing 6 M of urea, 2 M of
thiourea, 10 mM of dithiothreitol (DTT), 30 mM of TrisHCl pH 8.8 and 0.1% of Zwitterionic Acid
468 Labile Surfactant I (ZALS I, Protea Bioscience, Morgantown, USA). Protein powders were mixed
in the buffer using a metal spatula before vortexing the tubes for 3 min. Remaining cellular debris
470 were segregated from soluble proteins by centrifugation (12,500 rpm, 25 min, room temperature).
Protein concentrations were determined using the PlusOne 2-D Quant kit (GE Healthcare, Little
472 Chalfont, UK) and adjusted to 4 μ g. μ l⁻¹ prior to digestion.

Digestion was performed in 0.2 ml strip tubes from 10 μ l of diluted proteins. Proteins were
474 incubated one hour at room temperature for reduction by the 10 mM DTT present in the buffer.
Thereafter, proteins were alkylated one hour in 40 mM iodoacetamide (room temperature in the
476 dark) and diluted with 50 mM ammonium bicarbonate to decrease total urea and thiourea
concentration to 0.77 M. Overnight digestion was performed at 37°C with 1/50 (w/w) trypsin
478 (Promega, Charbonnières-les-Bains, France) and stopped by acidification (1% total volume of
trifluoroacetic acid, TFA). The resulting peptides were desalted on solid phase extraction using
480 polymeric C18 columns (strata XL 100 μ m, ref 8E-S043-TGB; Phenomenex, Le Pecq, France) as
follows. Peptides were first diluted in 3% ACN and 0.06% acetic acid in water (washing buffer) up
482 to a final volume of 500 μ l. Then, they were loaded onto cartridges previously conditioned with 500
 μ l of ACN and rinsed three times with 500 μ l of washing buffer. Peptides were rinsed three times
484 with 500 μ l of washing buffer and eluted twice by adding 300 μ l of 40% ACN and 0.06% acetic
acid. To finish, eluted peptides were speed-vac dried and suspended in a solution containing 2%
486 ACN, 0.05% TFA and 0.05 % formic acid.

488

490 **LC-MS/MS analyses**

Samples were analyzed by LC-MS/MS by batches of 96. Analyses were performed using a
492 NanoLC-Ultra System (nano2DUltra, Eksigent, Les Ulis, France) connected to a Q-Exactive mass
spectrometer (Thermo Electron, Waltham, MA, USA). A 400 ng of protein digest were loaded onto
494 a Biosphere C18 pre-column (0.3 × 5 mm, 100 Å, 5 µm; Nanoseparation, Nieuwkoop, Netherlands)
at 7.5 µl.min⁻¹ and desalted with 0.1% formic acid and 2% ACN. After 3 min, the precolumn was
496 connected to a Biosphere C18 nanocolumn (0.075 × 150 mm, 100 Å, 3 µm, Nanoseparation).
Buffers were 0.1% formic acid in water (A) and 0.1% formic acid and 100% ACN (B). Peptides
498 were separated using a linear gradient from 5 to 35% buffer B for 40 min at 300 nl.min⁻¹. One run
took 60 min, including the regeneration step at 95% buffer B and the equilibration step at 95%
500 buffer A.

Ionization was performed with a 1.4-kV spray voltage applied to an uncoated capillary
502 probe (10 µm tip inner diameter; New Objective, Woburn, MA, USA). Peptide ions were analyzed
using Xcalibur 2.2 (Thermo Electron) with the following data-dependent acquisition steps: (1) MS
504 scan (mass-to-charge ratio (m/z) 400 to 1400, 70,000 resolution, profile mode), (2) MS/MS (17,500
resolution, collision energy = 27%, profile mode). Step 2 was repeated for the eight major ions
506 detected in step 1 with a charge of 2 or 3. Dynamic exclusion was set to 40 s. Xcalibur raw datafiles
were transformed to mzXML open source format using msconvert software in the ProteoWizard
508 3.0.3706 package (Kessner et al. 2008). During conversion, MS and MS/MS data were centroided.

510 **Peptide and protein identification**

Peptide identifications were performed using the MaizeSequence genome database (Release
512 5a, 136,770 entries, <https://ftp.maiz gdb.org/MaizeGDB/FTP/>) supplemented with 1821 FV2

sequences showing presence/absence variations (Darracq et al. 2018) and with a custom database
514 containing standard contaminants. Database searches were performed using X!Tandem (Craig and
Beavis 2004) (version 2015.04.01.1) with the following main parameters. Enzymatic cleavage was
516 declared as a trypsin digestion with one possible misscleavage. Cystein carboxyamidomethylation
and methionine oxidation were set to static and possible modifications, respectively. Precursor mass
518 error was set to 10 ppm and fragment mass tolerance was set to 0.02 Da. In refine mode, a second
search was performed with the same settings, except that protein N-ter acetylation was added as a
520 potential modification and that the point mutations option was activated to detect possible single
amino acid changes in the peptide sequences. Only peptides with an E-value smaller than 0.01 were
522 reported.

Identified proteins were filtered and grouped using a homemade C++ version of X!
524 TandemPipeline (Langella et al. 2017) especially designed to handle hundreds of MS run files. Only
the proteins identified with a minimum of two peptides were considered as valid. Protein inference
526 was performed using all samples together. The false discovery rate (FDR) was assessed from
searches against a decoy database (using the reversed amino acid sequence for each protein) and
528 was estimated at 0.03% for peptides.

Functional annotation of proteins was based on MapMan mapping (Thimm et al. 2004;
530 Usadel et al. 2009) (Zm_B73_5b_FGS_cds_2012 available at <https://mapman.gabipd.org/>) and on a
custom KEGG classification build by manually attributing the MapMan bins to KEGG pathways
532 (Dillmann, pers. com.).

534 **Protein quantification**

Protein quantification was performed from the peptide data obtained after ion
536 chromatograms extraction and retention time (RT) alignment using MassChroQ software version
2.1.0 (Valot et al. 2011) with the following parameters: "ms2_1" alignment method,

538 tendency_halfwindow of 10, MS1 smoothing halfwindow of 0, MS2 smoothing halfwindow of 15,
"quant1" quantification method, XIC extraction based on max, min and max ppm range of 10, anti-
540 spike half of 5, background half median of 5, background half min max of 20, detection thresholds
on min and max at 30 000 and 50 000, respectively, peak post-matching mode, "ni min abundance"
542 of 0.1. Peptide data were filtered to remove the genotypes represented by only one or two samples
instead of the expected four as well as outliers samples for which we suspected technical problems
544 during sample preparation or MS analysis. At the end, the MS dataset included 977 samples.
Proteins were then quantified using two methods.

546 *XIC-based quantification.* Proteins were quantified based on peptide intensity data
processed as follows. We first removed the peptides ions showing standard deviations of retention
548 time >15 s, which may arise from mis-identifications. Intensity normalization was subsequently
performed to take into account possible global quantitative variations between LC-MS/MS runs.
550 For this, we used a local normalization method described in Millan-Oropeza *et al.* (2017). We then
removed the peptides shared between several proteins as well as the peptides for which both the
552 unmodified form and a mass modification corresponding to an amino acid change was detected by
the point mutation option of X!Tandem. These mutated peptide forms represent allelic versions of
554 the sequences present in the searched protein database. In heterozygous genotypes, each allelic
version produces its own MS signal, so that their measured intensities are not representative of the
556 total protein abundance. We also removed the peptide ions presenting more than 10% missing
values and those showing inconsistent intensity profiles. To this end, we computed Pearson
558 correlations between log-intensities averaged across replicates for each pair of peptide ions
belonging to the same protein. The peptide ion with the highest number of significant correlations
560 (P -value < 0.01 after adjustment for multiple testing (Benjamini and Hochberg 1995)) was chosen
as a reference for the protein. The peptide ions showing non-significant correlation to the reference
562 (adjusted P -value \geq 0.01) or whose coefficients of correlation to the reference were inferior to 0.3

were removed. To finish, we excluded the proteins quantified by only one peptide. As samples were
564 grouped by batches of 96 analyzed by LC-MS/MS over a period of several months, we observed a
strong batch effect on peptide normalized intensities. To correct this batch effect, we fitted a linear
566 model to log-transformed intensity data, including only batches, and we subtracted the component
due to the batch effects. Then, for each protein, we modeled the peptide data using the following
568 mixed-effects model derived from Blein-Nicolas *et al.* (2012):

$$I'_{ijkl} = \mu + G_j + E_k + (G \times E)_{jk} + R_{l(k)} + P_i + \theta_{jkl} + \varepsilon_{ijkl} \quad (1)$$

570 where I'_{ijkl} is the corrected, normalized log-intensity measured for peptide i in genotype j , watering
condition k and replicate l ;

572 μ is the mean intensity for a given protein;

G_j is the effect of the genotype j ;

574 E_k is the effect of the watering condition k ;

$(G \times E)_{jk}$ is the effect of the genotype j x watering condition k interaction;

576 $R_{l(k)}$ is the effect of the replicate l nested in the watering condition k ;

P_i is the effect of the peptide i ;

578 $\theta_{jkl} \sim \mathcal{N}(0, \sigma_\theta^2)$ is the random technical variation due to handling and injection in the mass
spectrometer of the sample jkl ;

580 $\varepsilon_{ijkl} \sim \mathcal{N}(0, \sigma_\varepsilon^2)$ is the residual error.

Model parameters were estimated by maximizing the restricted log-likelihood (REML method) and
582 the differential protein abundance analysis was performed by analysis of variance (ANOVA). The
resulting P -values were adjusted for multiple testing by the Benjamini-Hochberg procedure
584 (Benjamini and Hochberg 1995).

To subsequently perform GWAS at the protein level, we estimated protein abundances in each
586 watering condition using the following model:

$$I'_{ijkl} = \mu_k + G_{jk} + R_{lk} + P_{ik} + \theta_{jkl} + \varepsilon_{ijkl} \quad (2)$$

588 where μ_k is the mean intensity obtained for a given protein in the watering condition k ;

G_{jk} is the effect of the genotype j in the watering condition k ;

590 R_{lk} is the effect of the replicate l in the watering condition k ;

P_{ik} is the effect of the peptide i in the watering condition k .

592 Protein abundances were computed as adjusted means as follows:

$$A_{jk} = \mu_k + G_{jk} \quad (3)$$

594 *Peak counting (PC)-based quantification.* Proteins that could not be quantified based on
XIC because their peptides showed to many missing intensity values were quantified based on their
596 number of associated chromatographic peaks (*i.e.* quantified peptide ions). The shared peptides, the
peptide ions showing variable RT and the peptides for which a mass modification corresponding to
598 an amino acid change was detected were removed before computing protein abundances as peak
numbers. The proteins for which the peak counts < 2 in any of the samples were deleted.

600 Normalization was then performed as follows:

$$Anorm_{ps} = \frac{A_{ps}}{\sum_{n=1}^P A_{ns}} \times \frac{\sum_{m=1}^S \sum_{n=1}^P A_{nm}}{S} \quad (4)$$

602 where A_{ps} is the abundance of protein p in sample s ;

P is the number of quantified proteins;

604 S is the number of samples.

As mentioned above, we corrected the batch effect by fitting a linear model to square-root
606 transformed, normalized protein abundances, including only batches, and subtracting the
component due to the batch effects. We then used the following model to detect protein abundance
608 changes:

$$A'_{jkl} = \mu + G_j + E_k + (G \times E)_{jk} + \alpha_l + \epsilon_{jkl} \quad (5)$$

610 where A'_{jkl} is the corrected, normalized, square-root transformed abundance obtained for a given
protein in genotype j , watering condition k and replicate l ;

612 μ is the mean abundance for the protein;

G_j is the effect of the genotype j ;

614 E_k is the effect of the watering condition k ;

$(G \times E)_{jk}$ is the effect of the genotype j x watering condition k interaction;

616 $\alpha_l \sim \mathcal{N}(0, \sigma_\alpha^2)$ is the random effect of the replicate l ;

$\varepsilon_{ijkl} \sim \mathcal{N}(0, \sigma_\varepsilon^2)$ is the residual error.

618 Estimation of the model parameters, differential analysis and *P-value* adjustment were performed as
described above. Finally, for GWAS, we estimated the protein abundances separately in each
620 watering condition with a mixed model derived from (5) and including only a fixed effect of the
genotype and a random effect of the replicate. Protein abundances were computed as adjusted
622 means as in (3).

624 **Genome wide association study**

GWAS was performed on protein abundances estimated in each watering condition using the
626 single locus mixed model described in Yu *et al.* (2006). The variance-covariance matrix was
determined as described in Rincent *et al.* (2014) by a kinship matrix derived from all SNPs except
628 those on the chromosome containing the SNP being tested. The SNP effects were estimated by
generalized least squares and their significance was tested with an F-statistic. A SNP was considered
630 as significantly associated when $-\log_{10}(P\text{-value}) > 5$. A set of 961,971 SNPs obtained from lines
genotyping using a 50 K Infinium HD Illumina array (Ganal *et al.* 2011), a 600 K Axiom
632 Affymetrix array (Unterseer *et al.* 2014) and a set of 500 K SNPs obtained by genotyping by
sequencing (Negro *et al.*, in print) was tested. Analyses were performed with FaST-LMM (Lippert
634 *et al.* 2011) v2.07. Only SNPs with minor allele frequencies $> 5\%$ were considered.

Inflation factors were computed as the slopes of the linear regressions on the QQplots
636 between observed $-\log(P\text{-value})$ and expected $-\log(P\text{-value})$. Inflation factors were close to 1
(median of 1.08 and 1.05 in the XIC-based and PC-based sets, respectively), indicating low
638 inflation of $P\text{-values}$.

640 **Detection of QTLs from significantly associated SNPs**

Three different methods implemented in R (R core team 2013) version 3.3.3 were used to
642 summarize the significantly associated SNPs into pQTLs. *The genetic method*: two contiguous
SNPs were considered as belonging to a same QTL when the genetic distance separating them was
644 inferior to 0.1 cM. *The LD-based method*: two contiguous SNPs were considered as belonging to a
same QTL when their LD-based windows (Negro *et al.*, in print) overlapped. *The geometric*
646 *method*: for each chromosome, we ordered the SNPs according to their physical position. Then, we
smoothed the $-\log_{10}(P\text{-value})$ signal by computing the maximum of the $-\log_{10}(P\text{-values})$ in a
648 sliding window containing N consecutive SNPs. An association peak was detected when the
smoothed $-\log_{10}(P\text{-value})$ signal exceeded a max threshold M . Two consecutive peaks were
650 considered as two different QTLs when the $P\text{-value}$ signal separating them went below a min
threshold m . The parameters for QTL detection were fixed empirically at $N=500$, $M=5$ and $m=4$.
652 For the three methods described above, the position of a QTL was determined by the SNP
exhibiting the highest $-\log_{10}(P\text{-value})$. A pQTL was considered as local when located within 1 Mb
654 upstream or downstream the coding sequence of the gene encoding the corresponding protein.

656 **Complementary data analyses**

The following complementary data analyses were performed with R (R core team 2013)
658 version 3.3.3.

Broad sense heritability of protein abundance.

660 For each protein, the broad sense heritability of abundance was computed in each of the two
watering conditions as follows. For the proteins quantified by the XIC-based approach, abundances
662 were estimated in each sample as adjusted means from (1), by excluding the peptide effect P_{ik} and
the random sample effect Θ_{jkl} . For the proteins quantified by the PC-based approach, the corrected,
664 normalized, square-root transformed abundances were used. Protein abundances were then modeled
as follows:

$$666 \quad A_{jkl} = \mu_k + \beta_{jk} + \gamma_{kl} + \epsilon_{jkl} \quad (6)$$

where A_{jkl} is the abundance estimated for a given protein in the genotype j , the replicate i and the
668 watering condition k

$\beta_{jk} \sim \mathcal{N}(0, \sigma_\beta^2)$ is the random effect of the genotype j in the watering condition k

670 $\gamma_{kl} \sim \mathcal{N}(0, \sigma_\gamma^2)$ is the random effect of the replicate l in the watering condition k .

Heritability was subsequently computed as

$$672 \quad H^2 = \frac{\sigma_\beta^2}{(\sigma_\beta^2 + \sigma_\gamma^2 / N)} \quad (7)$$

where N is the number of replicates.

674 *Protein co-expression analysis*

Protein co-expression analysis was performed using the WGCNA R package (Langfelder and
676 Horvath 2008). Using a procedure developed to correct the LD by the structure and/or the
relatedness and implemented in the LDcorSV R package (Mangin et al. 2012), we computed pair-
678 wise Pearson's correlations corrected by structure and kinship ($|r_{corrected}|$) and used them as input
similarity matrix. The softpower parameter was set at 2. Adjacency and topological overlap matrices
680 were both unsigned. Protein modules were constituted with a minimum module size set at 20 and a
control over sensitivity splitting set at 4. The minimum height for merging modules was set at 0.25.
682 The other parameters were left at default values. Graphical representations of the resulting networks

were performed with Cytoscape (Shannon et al. 2003) v3.5.1 using an unweighted spring embedded
684 layout. Module eigengenes were computed as described in the WGCNA R package.

QTL co-localization

686 Co-localizations between QTLs were detected when they fulfilled two criteria. First, the LD-based
windows around the QTLs (Negro *et al.*, in print) should overlap. Second, the absolute value of the
688 Pearson's correlation of coefficient corrected by structure and kinship (the $|r_{corrected}|$ mentioned above)
between the values of the phenotypes controlled by the QTLs should be superior to 0.3. We
690 determined this value empirically, in absence of a statistical test to test the significance of the
corrected correlation.

Candidate genes identification

For each QTL/pQTL co-localization, gene accession present in the interval defined by the
694 intersection between the LD-based windows around the QTL and the pQTL were retrieved from the
MaizeSequence genome database (Release 5a). Low confidence gene models and transposable
696 elements were not considered.

698 DATA ACCESS

The raw MS output files were deposited online using PROTIcDb (Langella et al. 2007;
700 Ferry-Dumazet et al. 2005; Langella et al. 2013) at the following URL:
<http://moulon.inra.fr/protic/amaizing>. They are currently available with the following username:
702 reviewer and password: reviewer. They will be made freely available after publication. Detailed
information on the peptides and proteins identified in all LC-MS/MS runs as well as peptide
704 intensities and protein abundances obtained for each sample are also freely available on PROTIcDb
at the same URL.

706 Phenotypic data are available online using the PHIS information system (Neveu et al. 2019)
at the following URL: <http://www.phis.inra.fr/openphis/web/index.php?r=project>
708 [%2Fview&id=Systems+genetics+for+maize+drought+tolerance+%28Amaizing+project%29](http://www.phis.inra.fr/openphis/web/index.php?r=project). Leaf
area early was defined at the seven leaves stage, representing 24 d_{20°C} (thermal time in equivalent
710 days at 20°C). Leaf area late was defined at the 12 leaves stage, representing 45 d_{20°C}.

Genotyping data are available at the following URL: [https://data.inra.fr/privateurl.xhtml?](https://data.inra.fr/privateurl.xhtml?token=a0dbedde-249e-4808-9f51-51e2004678f7)
712 [token=a0dbedde-249e-4808-9f51-51e2004678f7](https://data.inra.fr/privateurl.xhtml?token=a0dbedde-249e-4808-9f51-51e2004678f7).

ACKNOWLEDGMENTS

714 This work was supported by the Agence Nationale de la Recherche project ANT-10-BTBR-01
(Amazing). Proteomics analyses were performed on the PAPPSO platform (<http://pappso.inra.fr>)
716 which is supported by INRA (<http://www.inra.fr>), the Ile-de-France regional council
(<https://www.iledefrance.fr/education-recherche>), IBiSA (<https://www.ibisa.net>) and SPS
718 (<https://www6.inra.fr/saclay-plant-sciences>). The authors want to thank Sylvie Coursol for her
critical reviewing of the manuscript, H el ene Corti for her help in sample preparation and Olivier
720 Langella for having specially developed a pipeline to upload the proteomics data on ProticDB. They
are also grateful to people from INRA LEPSE: Fran ois Tardieu for its participation to the
722 coordination of the plant experiment; Beno t Suard, Pauline Sidawi and Olivier Martin for their
technical assistance during the experiment; Santiago Alvarez Prado for his contribution to plant
724 traits and QTL analysis.

726 AUTHORS CONTRIBUTION

AC and MZ designed research; CW designed and coordinated the plant experiment in PhenoArch
728 and the genetic analysis of plant traits; LBC performed the plant experiment and analyzed image-
based phenotypic data; MBN and TB performed the proteomics experiments; SSN developed the
730 GWAS pipeline and performed the quality control on the genotyping; SDN performed the
genotyping and estimated local LD; MBN and MZ analyzed the proteomics data, MBN performed
732 the systems genetics study and wrote the manuscript. All authors discussed the results and read and
approved the final manuscript.

734

DISCLOSURE DECLARATION

736 The authors declare no competing interest.

738 REFERENCES

- Albert FW, Treusch S, Shockley AH, Bloom JS, Kruglyak L. 2014. Genetics of single-cell protein abundance variation in large yeast populations. *Nature* **506**: 494–497.
- Albertin W, Marullo P, Bely M, Aigle M, Bourgeois A, Langella O, Balliau T, Chevret D, Valot B, da Silva T, et al. 2013. Linking post-translational modifications and variation of phenotypic traits. *Mol Cell Proteomics* **12**: 720–735.
- Balliau T, Blein-Nicolas M, Zivy M. 2018. Evaluation of optimized tube-gel methods of sample preparation for large-scale plant proteomics. *Proteomes* **6**.
- Basnet RK, Del Carpio DP, Xiao D, Bucher J, Jin M, Boyle K, Fobert P, Visser RGF, Maliepaard C, Bonnema G. 2016. A systems genetics approach identifies gene regulatory networks associated with fatty acid composition in *Brassica rapa* seed. *Plant Physiol* **170**: 568–585.
- Battle A, Khan Z, Wang SH, Mitrano A, Ford MJ, Pritchard JK, Gilad Y. 2015. Impact of regulatory variation from RNA to protein. *Science* **347**: 664–667.
- Benjamini Y, Hochberg Y. 1995. Controlling the false discovery rate: A practical and powerful approach to multiple testing. *J R Stat Soc Ser B Methodol* **57**: 289–300.
- Blein-Nicolas M, Albertin W, da Silva T, Valot B, Balliau T, Masneuf-Pomarède I, Bely M, Marullo P, Sicard D, Dillmann C, et al. 2015. A systems approach to elucidate heterosis of protein abundances in yeast. *Mol Cell Proteomics* **14**: 2056–2071.
- Blein-Nicolas M, Xu H, de Vienne D, Giraud C, Huet S, Zivy M. 2012. Including shared peptides for estimating protein abundances: A significant improvement for quantitative proteomics. *Proteomics* **12**: 2797–2801.
- Bourgeois M, Jacquin F, Cassecuelle F, Savoies V, Belghazi M, Aubert G, Quillien L, Huart M, Marget P, Burstin J. 2011. A PQL (protein quantity loci) analysis of mature pea seed proteins identifies loci determining seed protein composition. *Proteomics* **11**: 1581–1594.
- Cabrera-Bosquet L, Fournier C, Briche N, Welcker C, Suard B, Tardieu F. 2016. High-throughput estimation of incident light, light interception and radiation-use efficiency of thousands of plants in a phenotyping platform. *New Phytol* **212**: 269–281.
- Campos H, Cooper M, Edmeades GO, Löffler CM, Schussler JR, Ibáñez M. 2006. Changes in drought tolerance in maize associated with fifty years of breeding for yield in the US Corn Belt. *Maydica* **51**: 369–381.
- Campos H, Cooper M, Habben JE, Edmeades GO, Schussler JR. 2004. Improving drought tolerance in maize: a view from industry *Field Crops Res* **90**: 19–34.
- Chaves MM, Maroco JP, Pereira JS. 2003. Understanding plant responses to drought — from genes to the whole plant. *Funct Plant Biol* **30**: 239–264.
- Chick JM, Munger SC, Simecek P, Huttlin EL, Choi K, Gatti DM, Raghupathy N, Svenson KL, Churchill GA, Gygi SP. 2016. Defining the consequences of genetic variation on a proteome-wide scale. *Nature* **534**: 500–505.
- Christie N, Myburg AA, Joubert F, Murray SL, Carstens M, Lin Y-C, Meyer J, Crampton BG, Christensen SA, Ntuli JF, et al. 2017. Systems genetics reveals a transcriptional network associated with susceptibility in the maize–grey leaf spot pathosystem. *Plant J* **89**: 746–763.
- Civelek M, Lusk AJ. 2014. Systems genetics approaches to understand complex traits. *Nat Rev Genet* **15**: 34–48.
- Cooper M, Gho C, Leafgren R, Tang T, Messina C. 2014. Breeding drought-tolerant maize hybrids for the US corn-belt: discovery to product. *J Exp Bot* **65**: 6191–6204.
- Craig R, Beavis RC. 2004. TANDEM: matching proteins with tandem mass spectra. *Bioinformatics* **20**: 1466–1467.

- Darracq A, Vitte C, Nicolas S, Duarte J, Pichon J-P, Mary-Huard T, Chevalier C, Bérard A, Le Paslier M-C, Rogowsky P, et al. 2018. Sequence analysis of European maize inbred line F2 provides new insights into molecular and chromosomal characteristics of presence/absence variants. *BMC Genomics* **19**.
- Daryanto S, Wang L, Jacinthe P-A. 2016. Global synthesis of drought effects on maize and wheat production. *PLoS ONE* **11**.
- de Vienne D, Leonardi A, Damerval C, Zivy M. 1999. Genetics of proteome variation for QTL characterization: application to drought-stress responses in maize. *J Exp Bot* **50**: 303–309.
- Feltus FA. 2014. Systems genetics: a paradigm to improve discovery of candidate genes and mechanisms underlying complex traits. *Plant Sci* **223**: 45–48.
- Feng S, Yue R, Tao S, Yang Y, Zhang L, Xu M, Wang H, Shen C. 2015. Genome-wide identification, expression analysis of auxin-responsive GH3 family genes in maize (*Zea mays* L.) under abiotic stresses. *J Integr Plant Biol* **57**: 783–795.
- Ferry-Dumazet H, Houel G, Montalent P, Moreau L, Langella O, Negroni L, Vincent D, Lalanne C, de Daruvar A, Plomion C, et al. 2005. PROTIcDb: A web-based application to store, track, query, and compare plant proteome data. *Proteomics* **5**: 2069–2081.
- Forestan C, Aiese Cigliano R, Farinati S, Lunardon A, Sanseverino W, Varotto S. 2016. Stress-induced and epigenetic-mediated maize transcriptome regulation study by means of transcriptome reannotation and differential expression analysis. *Sci Rep* **6**: 30446.
- Foss EJ, Radulovic D, Shaffer SA, Goodlett DR, Kruglyak L, Bedalov A. 2011. Genetic variation shapes protein networks mainly through non-transcriptional mechanisms. *PLoS Biol* **9**: e1001144.
- Ganal MW, Durstewitz G, Polley A, Bérard A, Buckler ES, Charcosset A, Clarke JD, Graner E-M, Hansen M, Joets J, et al. 2011. A large maize (*Zea mays* L.) SNP genotyping array: Development and germplasm genotyping, and genetic mapping to compare with the B73 reference genome. *PLoS ONE* **6**: e28334.
- Ghazalpour A, Bennett B, Petyuk VA, Orozco L, Hagopian R, Mungrue IN, Farber CR, Sinsheimer J, Kang HM, Furlotte N, et al. 2011. Comparative analysis of proteome and transcriptome variation in mouse. *PLoS Genet* **7**: e1001393.
- Goldman AD, Samudrala R, Baross JA. 2010. The evolution and functional repertoire of translation proteins following the origin of life. *Biol Direct* **5**: 15.
- Golldack D, Li C, Mohan H, Probst N. 2014. Tolerance to drought and salt stress in plants: Unraveling the signaling networks. *Front Plant Sci* **5**.
- Harrison MT, Tardieu F, Dong Z, Messina CD, Hammer GL. 2014. Characterizing drought stress and trait influence on maize yield under current and future conditions. *Glob Change Biol* **20**: 867–878.
- Johnson MR, Behmoaras J, Bottolo L, Krishnan ML, Pernhorst K, Santoscoy PLM, Rossetti T, Speed D, Srivastava PK, Chadeau-Hyam M, et al. 2015. Systems genetics identifies Sestrin 3 as a regulator of a proconvulsant gene network in human epileptic hippocampus. *Nat Commun* **6**: 6031.
- Keshishian H, Burgess MW, Specht H, Wallace L, Clauser KR, Gillette MA, Carr SA. 2017. Quantitative, multiplexed workflow for deep analysis of human blood plasma and biomarker discovery by mass spectrometry. *Nat Protoc* **12**: 1683–1701.
- Kessner D, Chambers M, Burke R, Agus D, Mallick P. 2008. ProteoWizard: open source software for rapid proteomics tools development. *Bioinformatics* **24**: 2534–2536.
- Langella O, Valot B, Balliau T, Blein-Nicolas M, Bonhomme L, Zivy M. 2017. X!TandemPipeline: A tool to manage sequence redundancy for protein inference and phosphosite identification. *J Proteome Res* **16**: 494–503.

- Langella O, Valot B, Jacob D, Balliau T, Flores R, Hoogland C, Joets J, Zivy M. 2013. Management and dissemination of MS proteomic data with PROTiCdb: example of a quantitative comparison between methods of protein extraction. *Proteomics* **13**: 1457–1466.
- Langella O, Zivy M, Joets J. 2007. The PROTiCdb database for 2-DE proteomics. *Methods Mol Biol* **355**: 279–303.
- Langfelder P, Horvath S. 2008. WGCNA: an R package for weighted correlation network analysis. *BMC Bioinformatics* **9**: 559.
- Li S-B, Xie Z-Z, Hu C-G, Zhang J-Z. 2016. A review of auxin response factors (ARFs) in plants. *Front Plant Sci* **7**.
- Lippert C, Listgarten J, Liu Y, Kadie CM, Davidson RI, Heckerman D. 2011. FaST linear mixed models for genome-wide association studies. *Nat Methods* **8**: 833–835.
- Lobell DB, Roberts MJ, Schlenker W, Braun N, Little BB, Rejesus RM, Hammer GL. 2014. Greater sensitivity to drought accompanies maize yield increase in the U.S. midwest. *Science* **344**: 516–519.
- Mähler N, Wang J, Terebieniec BK, Ingvarsson PK, Street NR, Hvidsten TR. 2017. Gene co-expression network connectivity is an important determinant of selective constraint. *PLoS Genet* **13**: e1006402.
- Mangin B, Siberchicot A, Nicolas S, Doligez A, This P, Cierco-Ayrolles C. 2012. Novel measures of linkage disequilibrium that correct the bias due to population structure and relatedness. *Heredity* **108**: 285–291.
- Mao H-D, Yu L-J, Li Z-J, Yan Y, Han R, Liu H, Ma M. 2016. Genome-wide analysis of the SPL family transcription factors and their responses to abiotic stresses in maize. *Plant Gene* **6**: 1–12.
- Markowitz F, Boutros M. 2015. An introduction to systems genetics. In *Systems Genetics* (eds. F. Markowitz and M. Boutros), pp. 1–11, Cambridge University Press, doi:10.1017/CBO9781139012751.001
- Meng Q, Chen X, Lobell DB, Cui Z, Zhang Y, Yang H, Zhang F. 2016. Growing sensitivity of maize to water scarcity under climate change. *Sci Rep* **6**: 19605.
- Millan-Oropeza A, Henry C, Blein-Nicolas M, Aubert-Frambourg A, Moussa F, Bleton J, Virolle M-J. 2017. Quantitative proteomics analysis confirmed oxidative metabolism predominates in *Streptomyces coelicolor* versus glycolytic metabolism in *Streptomyces lividans*. *J Proteome Res* **16**: 2597–2613.
- Millet EJ, Welcker C, Kruijer W, Negro S, Coupel-Ledru A, Nicolas SD, Laborde J, Bauland C, Praud S, Ranc N, et al. 2016. Genome-wide analysis of yield in Europe: Allelic effects vary with drought and heat scenarios. *Plant Physiol* **172**: 749–764.
- Mizrachi E, Verbeke L, Christie N, Fierro AC, Mansfield SD, Davis MF, Gjersing E, Tuskan GA, Montagu MV, Peer YV de, et al. 2017. Network-based integration of systems genetics data reveals pathways associated with lignocellulosic biomass accumulation and processing. *Proc Natl Acad Sci* **114**: 1195–1200.
- Moreno-Moral A, Petretto E. 2016. From integrative genomics to systems genetics in the rat to link genotypes to phenotypes. *Dis Model Mech* **9**: 1097–1110.
- Munkvold JD, Laudencia-Chinguanco D, Sorrells ME. 2013. Systems genetics of environmental response in the mature wheat embryo. *Genetics* **194**: 265–277.
- Nadeau JH, Dudley AM. 2011. Systems genetics. *Science* **331**: 1015–1016.
- Nelson N, Junge W. 2015. Structure and energy transfer in photosystems of oxygenic photosynthesis. *Annu Rev Biochem* **84**: 659–683.
- Neveu P, Tireau A, Hilgert N, Nègre V, Mineau-Cesari J, Brichet N, Chapis R, Sanchez I, Pommier C, Charnomordic B, et al. 2019. Dealing with multi-source and multi-scale information in plant phenomics: the ontology-driven Phenotyping Hybrid Information System. *New Phytol* **221**: 588–601.

- Ogura T, Busch W. 2016. Genotypes, networks, phenotypes: Moving toward plant systems genetics. *Annu Rev Cell Dev Biol* **32**: 103–126.
- Orozco LD, Bennett BJ, Farber CR, Ghazalpour A, Pan C, Che N, Wen P, Qi HX, Mutukulu A, Siemers N, et al. 2012. Unraveling inflammatory responses using systems genetics and gene-environment interactions in macrophages. *Cell* **151**: 658–670.
- Osakabe Y, Osakabe K, Shinozaki K, Tran L-SP. 2014. Response of plants to water stress. *Front Plant Sci* **5**.
- Popadin KY, Gutierrez-Arcelus M, Lappalainen T, Buil A, Steinberg J, Nikolaev SI, Lukowski SW, Bazykin GA, Seplyarskiy VB, Ioannidis P, et al. 2014. Gene age predicts the strength of purifying selection acting on gene expression variation in humans. *Am J Hum Genet* **95**: 660–674.
- Prado SA, Cabrera-Bosquet L, Grau A, Coupel-Ledru A, Millet EJ, Welcker C, Tardieu F. 2018. Phenomics allows identification of genomic regions affecting maize stomatal conductance with conditional effects of water deficit and evaporative demand. *Plant Cell Environ* **41**: 314–326.
- Preston JC, Hileman LC. 2013. Functional Evolution in the Plant SQUAMOSA-PROMOTER BINDING PROTEIN-LIKE (SPL) Gene Family. *Front Plant Sci* **4**: 80.
- R core team. 2013. R: A language and environment for statistical computing. R Foundation for Statistical Computing, Vienna, Austria.
- Rincent R, Moreau L, Monod H, Kuhn E, Melchinger AE, Malvar RA, Moreno-Gonzalez J, Nicolas S, Madur D, Combes V, et al. 2014. Recovering power in association mapping panels with variable levels of linkage disequilibrium. *Genetics* **197**: 375–387.
- Seki M, Umezawa T, Urano K, Shinozaki K. 2007. Regulatory metabolic networks in drought stress responses. *Curr Opin Plant Biol* **10**: 296–302.
- Shang Y, Yan L, Liu Z-Q, Cao Z, Mei C, Xin Q, Wu F-Q, Wang X-F, Du S-Y, Jiang T, et al. 2010. The Mg-chelatase H subunit of Arabidopsis antagonizes a group of WRKY transcription repressors to relieve ABA-responsive genes of inhibition. *Plant Cell* **22**: 1909–1935.
- Shannon P, Markiel A, Ozier O, Baliga NS, Wang JT, Ramage D, Amin N, Schwikowski B, Ideker T. 2003. Cytoscape: a software environment for integrated models of biomolecular interaction networks. *Genome Res* **13**: 2498–2504.
- Shiferaw B, Prasanna BM, Hellin J, Bänziger M. 2011. Crops that feed the world 6. Past successes and future challenges to the role played by maize in global food security. *Food Secur* **3**: 307.
- Song K, Kim HC, Shin S, Kim K-H, Moon J-C, Kim JY, Lee B-M. 2017. Transcriptome analysis of flowering time genes under drought stress in maize leaves. *Front Plant Sci* **8**.
- Tardieu F, Simonneau T, Muller B. 2018. The physiological basis of drought tolerance in crop plants: A scenario-dependent probabilistic approach. *Annu Rev Plant Biol* **69**: 733–759.
- Thimm O, Bläsing O, Gibon Y, Nagel A, Meyer S, Krüger P, Selbig J, Müller LA, Rhee SY, Stitt M. 2004. Mapman: a user-driven tool to display genomics data sets onto diagrams of metabolic pathways and other biological processes. *Plant J* **37**: 914–939.
- Tripathi P, Rabara RC, Rushton PJ. 2014. A systems biology perspective on the role of WRKY transcription factors in drought responses in plants. *Planta* **239**: 255–266.
- Unterseer S, Bauer E, Haberer G, Seidel M, Knaak C, Ouzunova M, Meitinger T, Strom TM, Fries R, Pausch H, et al. 2014. A powerful tool for genome analysis in maize: development and evaluation of the high density 600 k SNP genotyping array. *BMC Genomics* **15**: 823.

- Usadel B, Poree F, Nagel A, Lohse M, Czedik-Eysenberg A, Stitt M. 2009. A guide to using MapMan to visualize and compare omics data in plants: a case study in the crop species, maize. *Plant Cell Environ* **32**: 1211–1229.
- Valliyodan B, Nguyen HT. 2006. Understanding regulatory networks and engineering for enhanced drought tolerance in plants. *Curr Opin Plant Biol* **9**: 189–195.
- Valot B, Langella O, Nano E, Zivy M. 2011. MassChroQ : A versatile tool for mass spectrometry quantification. *Proteomics* **11**: 3572–3577.
- van der Sijde MR, Ng A, Fu J. 2014. Systems genetics: From GWAS to disease pathways. *Biochim Biophys Acta* **1842**: 1903–1909.
- Vogel C, Marcotte EM. 2012. Insights into the regulation of protein abundance from proteomic and transcriptomic analyses. *Nat Rev Genet* **13**: 227–232.
- Wasinger VC, Zeng M, Yau Y. 2013. Current Status and Advances in Quantitative Proteomic Mass Spectrometry. *Int J Proteomics* 2013:180605
- Williams EG, Wu Y, Jha P, Dubuis S, Blattmann P, Argmann CA, Houten SM, Amariuta T, Wolski W, Zamboni N, et al. 2016. Systems proteomics of liver mitochondria function. *Science* **352**: aad0189.
- Yu J, Pressoir G, Briggs WH, Vroh Bi I, Yamasaki M, Doebley JF, McMullen MD, Gaut BS, Nielsen DM, Holland JB, et al. 2006. A unified mixed-model method for association mapping that accounts for multiple levels of relatedness. *Nat Genet* **38**: 203–208.
- Zhang J, Yang J-R. 2015. Determinants of the rate of protein sequence evolution. *Nat Rev Genet* **16**: 409–420.
- Zhang X, Liu X, Zhang D, Tang H, Sun B, Li C, Hao L, Liu C, Li Y, Shi Y, et al. 2017. Genome-wide identification of gene expression in contrasting maize inbred lines under field drought conditions reveals the significance of transcription factors in drought tolerance. *PLoS ONE* **12**: e0179477.
- Zipper SC, Qiu J, Kucharik CJ. 2016. Drought effects on US maize and soybean production: spatiotemporal patterns and historical changes. *Environ Res Lett* **11**: 094021.

740 **FIGURE LEGENDS**

Figure 1. Effect of a mild water deficit on the proteome. (A) Heatmap representations of the
742 abundances estimated for the XIC-based protein set (left) and the PC-based protein set (right). Each
line corresponds to a protein and each column to a genotype x watering condition combination. For
744 each protein, abundance values were scaled and represented by a color code as indicated by the
color-key bar. Hierarchical clusterings of the genotype x watering condition combinations (top) and
746 of the proteins (left) were built by using 1-the Pearson correlation coefficient as distance and the
unweighted pair group method with arithmetic mean (UPGMA) as aggregation method. (B)
748 Functions of the 200 most induced and 200 most repressed proteins under water deficit. (C)
Abundance profiles of the RAB17 dehydrin (GRMZM2G079440 quantified based on the number of
750 chromatographic peaks) and of a LEA protein (GRMZM2G352415 quantified based on peptide
intensities) in the two watering conditions. Genotypes on the x axis were ordered according to the
752 WD/WW abundance ratio.

754 **Figure 2. Relationship between the mean number of pQTLs per KEGG category and the
mean heritability per KEGG category.**

756

Figure 3. Distribution of pQTLs along the genome. (A) In the well-watered condition. (B) In the
758 water-deficit condition. Each point indicates the number of proteins controlled by a pQTL located in
a given genomic region defined by the linkage disequilibrium interval around a SNP. Dashed
760 horizontal lines indicate the arbitrary threshold used to detect pQTL hotspots. Names and positions
of the pQTL hotspots are indicated above each graph. Names in bold indicate the pQTL hotspots
762 confidently detected as potential pleiotropic loci (see Sup. Table 3 for details).

764 **Figure 4. Graphical representation of the co-expression networks resulting from the WGCNA**
analyses. Only proteins showing adjacencies > 0.02 are shown. The consensus network contains the
766 proteins that were co-expressed in the two watering conditions. The three views were created by
Cytoscape v3.5.1 using an unweighted, spring-embedded layout. The colors displayed on each
768 network represent the different modules identified by WGCNA. Functional enrichments of modules
are indicated in grey boxes. Condition-specific modules are surrounded by dashed circles.

770

Figure 5. Genomic positions of the co-localizing pQTLs, coQTLs and QTLs. The positions of
772 the nine pQTL hotspots robustly identified as potential loci with pleiotropic effects are indicated as
well as the position of the most promising candidate genes. Chromosomes are segmented in 1 Mb
774 bins. Grey dots represent the centromeres and blue dots indicate the position of genomic regions
showing evidences for pleiotropy both at the proteome and phenotype level. Blue lines indicate
776 pQTLs, coQTLs and QTLs that are determined by a same SNP.

* consensus module, ° WD-specific module

778

Figure 6. Identification of genomic regions involved in multi-scale genetic control.

780 (A) Distribution of the distances between co-localizing QTLs and pQTLs. (B) Detailed view of the
QTL, pQTL, coQTL detected in the region covered by the hotspot Hs52d on chromosome 5. Dots
782 represent the SNPs determining the position of the QTLs and horizontal bars represent the linkage
disequilibrium-based window around each SNP. Black circled dots indicate the pQTLs that co-
784 localize with QTLs or coQTLs with high correlations between the protein abundance and the
phenotypic trait value or the module eigengene. Vertical dashed lines indicate the position of SNPs
786 S5_88793314 (on the left) and AX-91658235 (on the right). The position of two transcription
factors (a SBP gene, GRMZM2G111136, and a C2C2-CO-like transcription factor,
788 GRMZM2G148772) representing promising candidate genes are indicated.

TABLES

790 **Table 1. Proteins associated to pQTLs co-localizing with QTLs.**

| Protein ID | Gene accession | Plaza 4.0 annotation ^a | # of QTL/pQTL co-localizations | Phenotypic trait |
|-----------------------|--------------------------------|---------------------------------------------------------------|--------------------------------|-------------------|
| a3.a1 | GRMZM2G306345 | pyruvate orthophosphate dikinase1 | 1 ^c | BI |
| c111.a2 | GRMZM2G085054 | Glycosyltransferase benzoxazinone synthesis 8 | 1 | WU |
| c135.a1 | GRMZM2G085577 | Alpha-1,4 glucan phosphorylase | 1 | LAI |
| c177.a1 | GRMZM2G027875 | Aminopeptidase M1 | 1 | LAI |
| c236.a1 ^b | GRMZM2G130230 | Glucose-6-phosphate dehydrogenase | 1 | LAI |
| c263.a1 | GRMZM2G162486 | Glutathione S-transferase | 1 | LAI |
| c264.a1 | GRMZM2G061969 | Phospholipase D | 1 | LAI |
| c291.a1 | GRMZM2G064799 | Succinate dehydrogenase 1 | 1 | LAI |
| c317.a1 | GRMZM2G134256 | Transaldolase 2 | 1 | LAI |
| c364.a1 ^b | GRMZM2G075624 GRMZM2G108474 | Translationally controlled tumor protein | 1 | gs |
| c513.a2 | GRMZM2G134668 | Calnexin | 1 | WU |
| c517.a1 | AC198418.3 | RNA helicase4 | 1 | LAI |
| c547.a1 | GRMZM2G033641 | Patellin-1 (SEC14-like protein) | 1 | LAI |
| c561.a1 ^b | GRMZM2G048085 | Senescence-associated protein DIN1 | 1 | Trate |
| c587.a1 ^b | GRMZM2G051677 | Fructokinase-2 | 1 | LAI |
| c607.a1 ^b | GRMZM2G352415 | Late embryogenesis abundant (LEA) protein | 1 | LAI |
| c739.a1 ^b | GRMZM2G085967 | Peroxidase | 1 | LAI |
| c790.a1 | GRMZM2G332976 | short chain alcohol dehydrogenase1 | 1 ^c | BI |
| c914.a2 | GRMZM2G373522 | Dehydrin | 1 | WU |
| c959.a2 ^b | GRMZM2G479423 | Aldose reductase | 1 | LAI |
| c976.a1 | GRMZM2G064360 | Basic endochitinase 1 | 1 | LAI |
| d1139.a1 ^b | GRMZM2G169207 | IMP dehydrogenase | 1 | LAI |
| d1261.a1 | GRMZM2G026800 | Probable plastid lipid-associated protein 10 | 1 | BI |
| d1513.a1 | GRMZM2G094712 | Aspartate aminotransferase | 1 | BI |
| d1624.a1 | GRMZM2G022563 | oxoacyl-[acyl-carrier-protein] synthase 3 | 1 | LAI |
| b33.a2 | GRMZM2G112165 | Heat shock protein 90-2 | 2 | Lal, WU |
| c178.a1 | GRMZM2G055489 | Sucrose-phosphatase 1 (ZmSPP1) | 2 | gs, Trate |
| c395.a1 | GRMZM2G165901 | Glycine-rich RNA-binding, ABA-inducible protein | 2 | BI, WU |
| c490.a1 | GRMZM2G038494 | Obg-like ATPase 1, GTP-binding protein-related | 2 | LAI |
| c997.a1 | GRMZM2G051943 | Endochitinase A | 2 | Lal, WU |
| d1066.a1 | GRMZM2G704005 | Lactoylglutathione lyase / glyoxalase I family protein | 2 | LAI |
| d1218.a1 ^b | GRMZM2G169516 | Indole-3-glycerol phosphate synthase | 2 | LAI |
| c144.a1 ^b | GRMZM2G120304 | hydroxyproline-rich glycoprotein family protein | 3 | Lal, WU |
| c654.a1 | GRMZM2G110567 | Protein binding, zinc finger family protein | 3 | LAI |
| c778.a1 | GRMZM2G017110 | Glutamate decarboxylase | 3 | WU, WUE |
| d1404.a1 | GRMZM2G080724 | 25.3 kDa heat shock protein | 3 | BI, Lal, WU |
| d1140.a1 ^b | GRMZM2G073079 GRMZM2G076348 | alpha/beta-Hydrolases superfamily protein | 4 | Lal, WU |
| d1512.a1 ^b | GRMZM5G815098 | Unknow | 4 | LAI |
| b94.a2 | GRMZM5G851266 | Putative polyphenol oxidase family protein | 5 | BI, Lal, WU |
| c115.a2 | GRMZM5G813217 | Heat shock protein 90-5 | 6 | BI, Lal, WU |
| d1161.a1 | GRMZM2G079440 | Dehydrin DHN1 (RAB-17 protein) | 7 | BI, gs, Trate, WU |
| c880.a1 | GRMZM2G176998 | Putative WD40-like beta propeller repeat family protein | 8 | BI, Lal, WU |

792 a Functions in bold are related to drought- or stress-response.

b Protein ID corresponding to different isoforms or accessions

794 c QTL/pQTL co-localization observed in the WW condition.

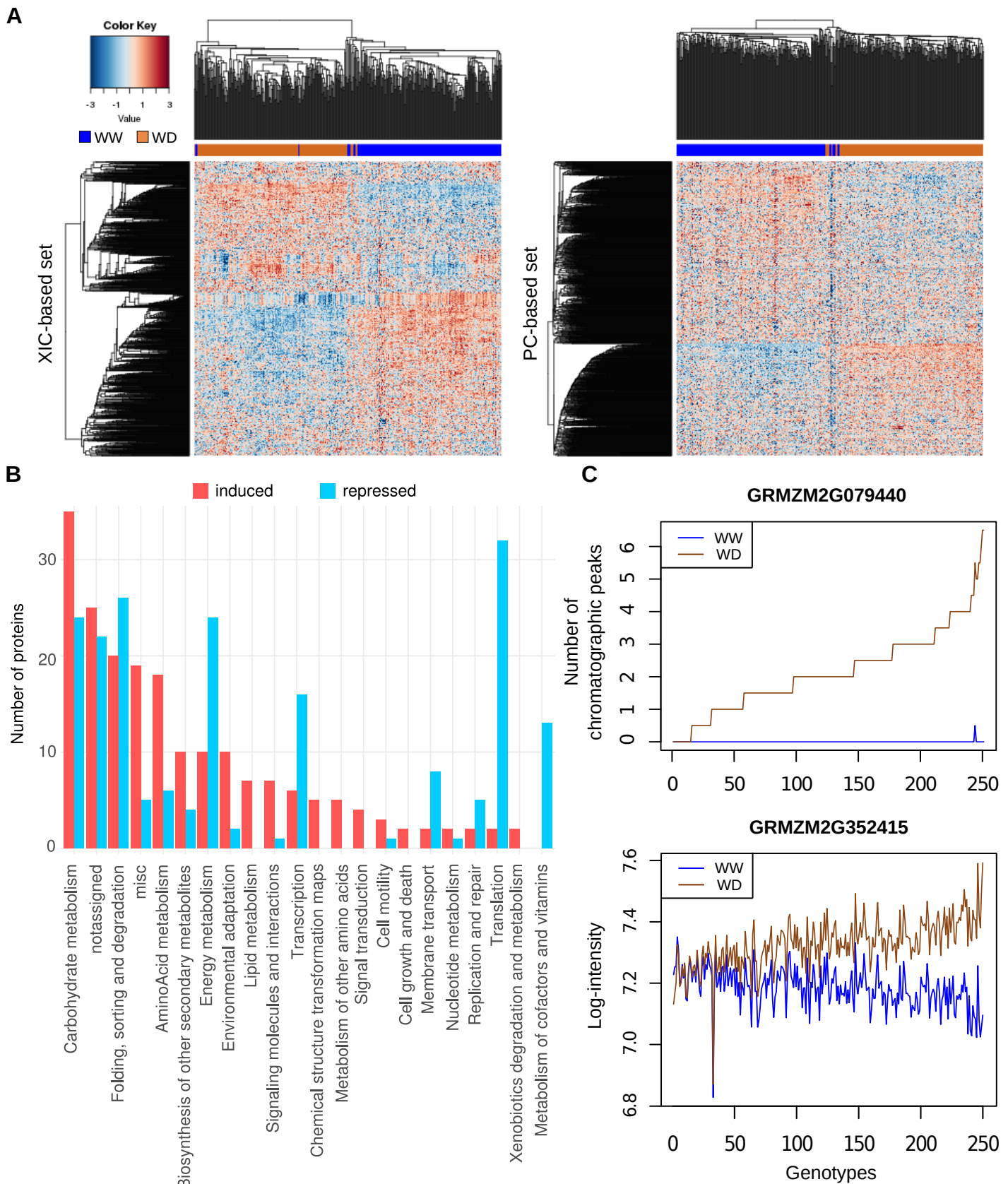


Figure 1. Effect of a mild water deficit on the proteome. (A) Heatmap representations of the abundances estimated for the XIC-based protein set (left) and the PC-based protein set (right). Each line corresponds to a protein and each column to a genotype x watering condition combination. For each protein, abundance values were scaled and represented by a color code as indicated by the color-key bar. Hierarchical clusterings of the genotype x watering condition combinations (top) and of the proteins (left) were built by using the 1-Pearson correlation coefficient as distance and the unweighted pair group method with arithmetic mean (UPGMA) as aggregation method. (B) Functions of the 200 most induced and 200 most repressed proteins under water deficit. (C) Abundance profiles of the RAB17 dehydrin (GRMZM2G079440 quantified based on the number of chromatographic peaks) and of a LEA protein (GRMZM2G352415 quantified based on peptide intensities) in the two watering conditions. Genotypes on the x axis were ordered according to the WD/WW abundance ratio.

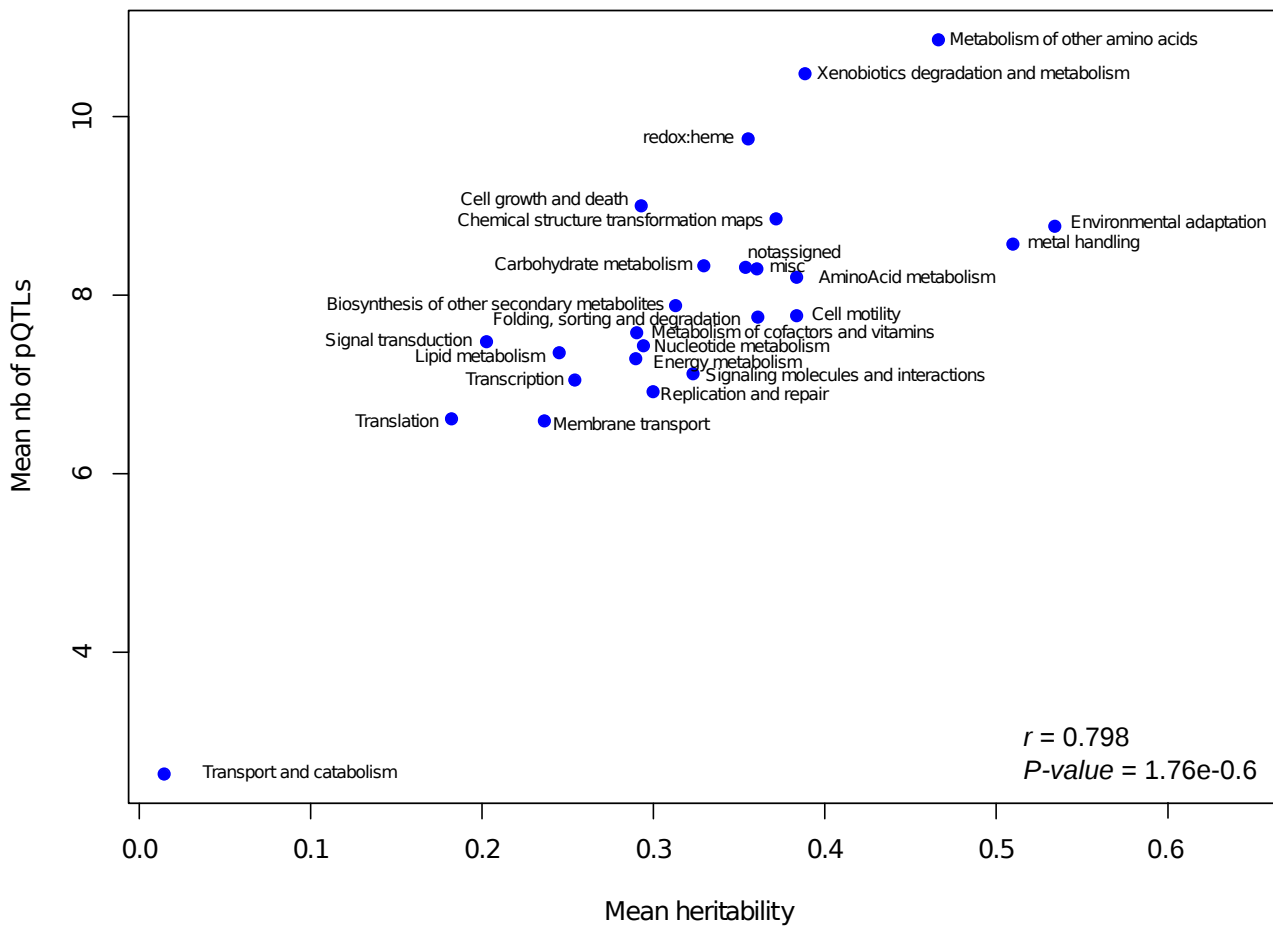


Figure 2. Relationship between the mean number of pQTLs per KEGG category and the mean heritability per KEGG category.

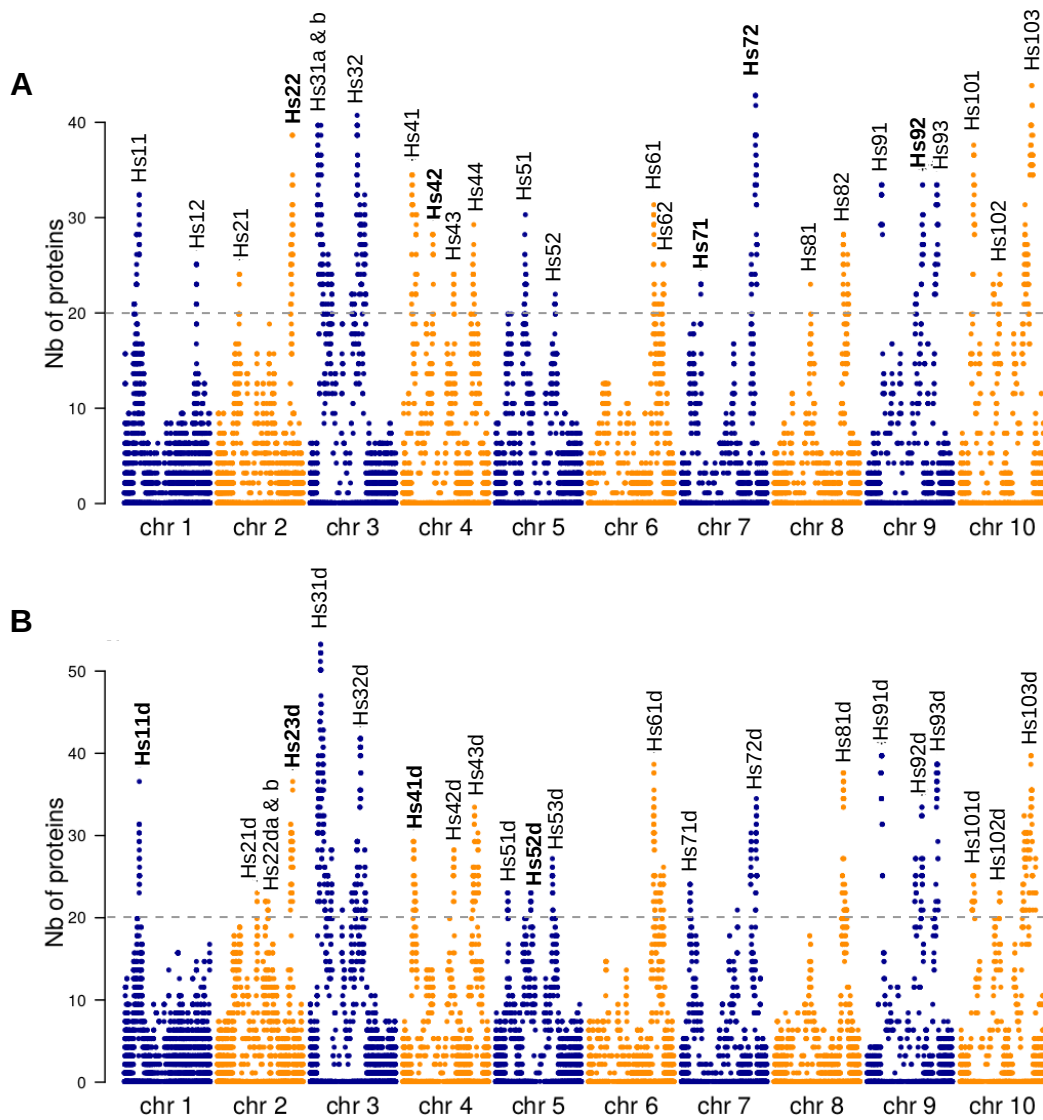
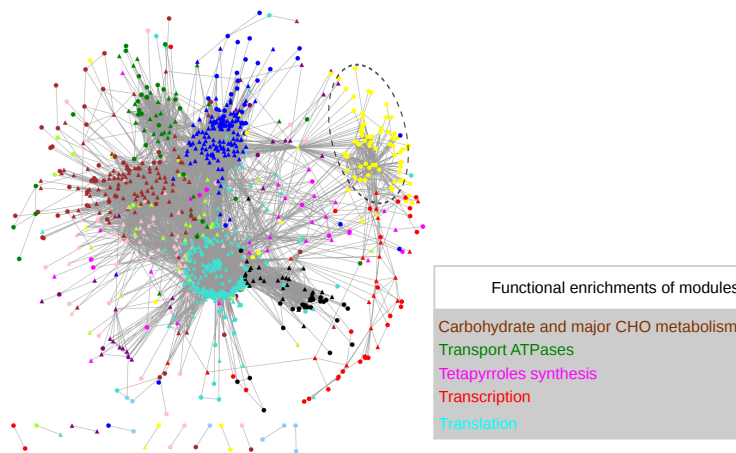
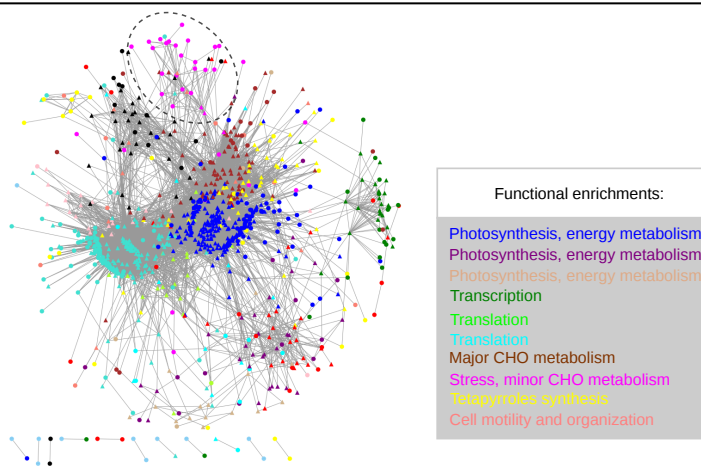


Figure 3. Distribution of pQTLs along the genome. (A) In the well-watered condition. (B) In the water deficit condition. Each point indicates the number of proteins controlled by a pQTL located in a given genomic region defined by the linkage disequilibrium interval around a SNP. Dashed horizontal lines indicate the arbitrary threshold used to detect pQTL hotspots. Names and positions of the pQTL hotspots are indicated above each graph. Names in bold indicate pQTL hotspots confidently detected as potential pleiotropic loci (see Sup. Table 3 for details).

WW network



WD network



Consensus network

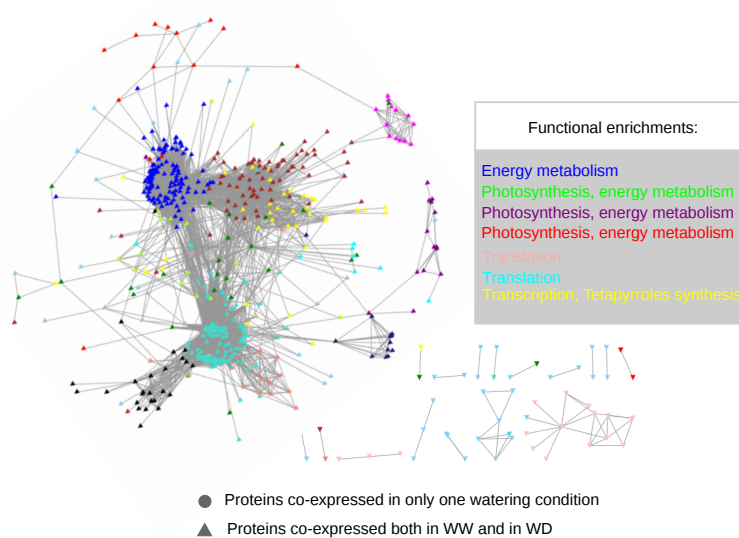


Figure 4. Graphical representation of the co-expression networks resulting from the WGCNA analyses. Only proteins showing adjacencies > 0.02 are shown. The consensus network contains the proteins that were co-expressed in the two watering conditions. The three views were created by Cytoscape v3.5.1 using an unweighted, spring-embedded layout. The colors displayed on each network represent the different modules identified by WGCNA. Functional enrichments of modules are indicated in grey boxes. Condition-specific modules are surrounded by dashed circles.

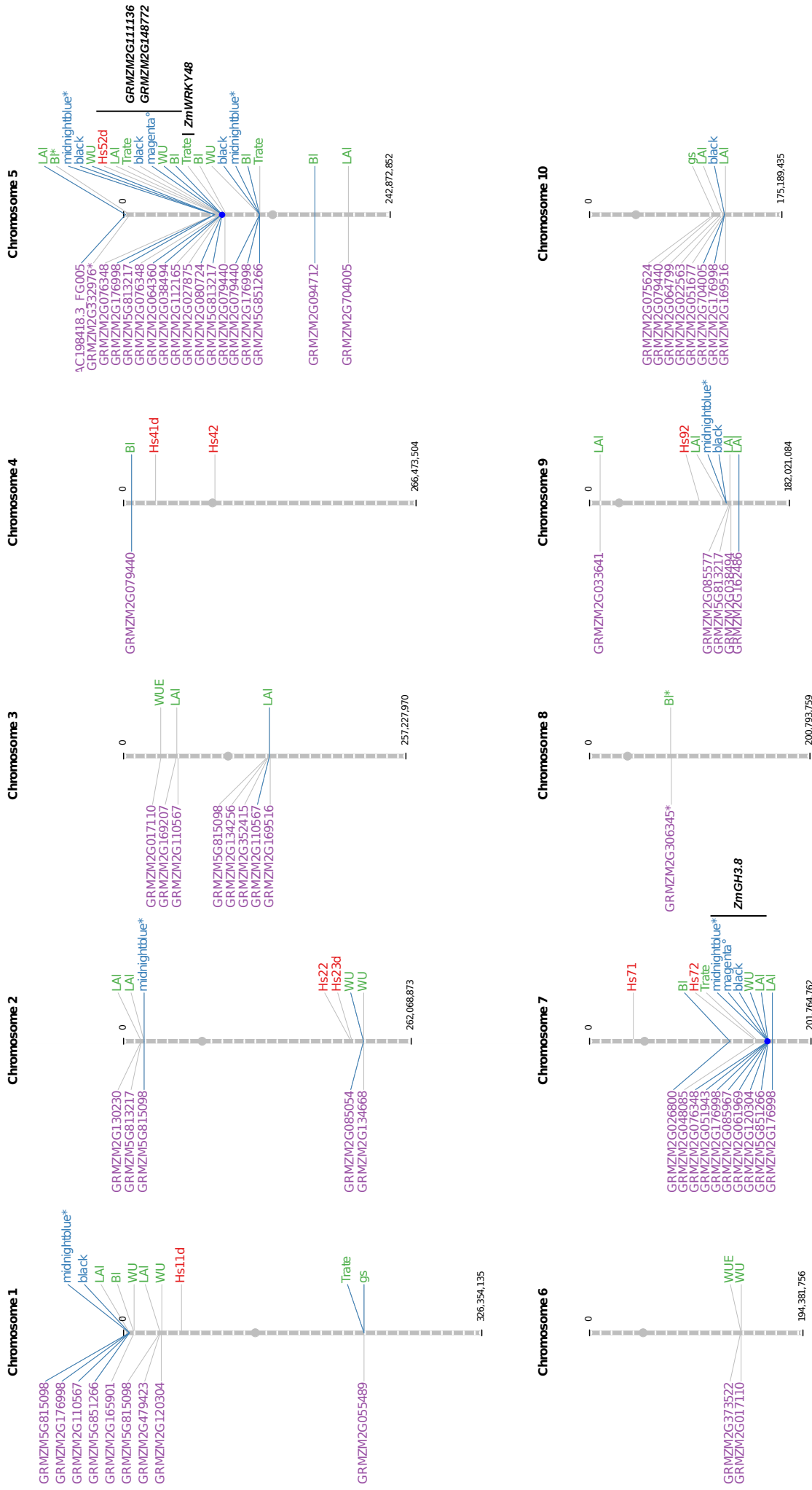


Figure 5. Genomic positions of the co-localizing pQTLs, coQTLs and QTLs. The positions of the nine pQTL hotspots robustly identified as potential loci with pleiotropic effects are indicated as well as the position of the most promising candidate genes. Chromosomes are segmented in 1 Mb bins. Grey dots represent the centromeres and blue dots indicate the position of genomic regions showing evidences for pleiotropy both at the proteome and phenotype level. Blue lines indicate pQTLs, coQTLs and QTLs that are determined by a same SNP. * consensus module, ° WD-specific module

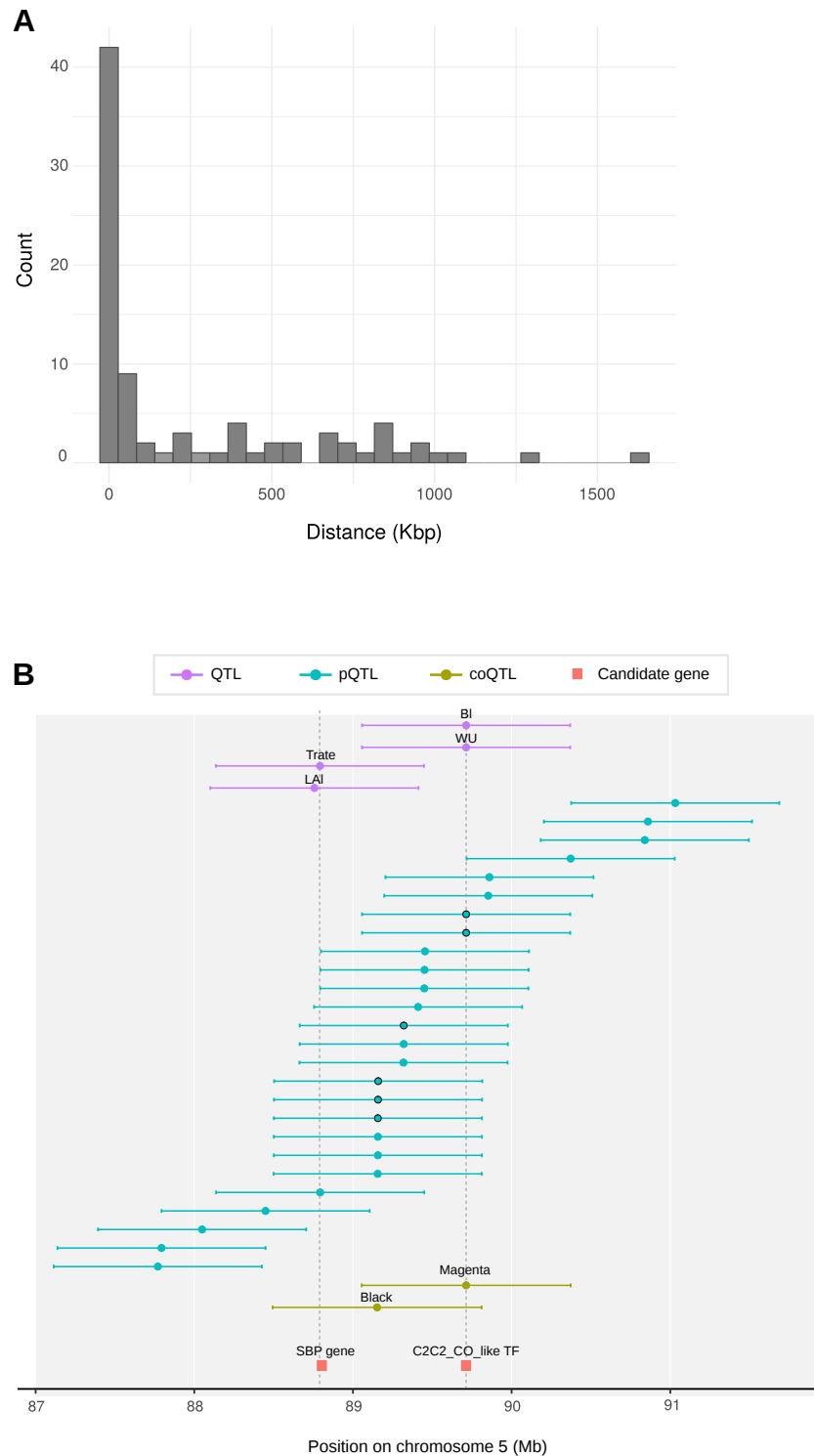


Figure 6. Identification of genomic regions involved in multi-scale genetic control.

(A) Distribution of the distances between co-localizing QTLs and pQTLs. (B) Detailed view of the QTL, pQTL, coQTL detected in the region covered by the hotspot Hs52d on chromosome 5. Dots represent the SNPs determining the position of the QTLs and horizontal bars represent the linkage disequilibrium-based window around each SNP. Black circled dots indicate the pQTLs that co-localize with QTLs or coQTLs with high correlations between the protein abundance and the phenotypic trait value or the module eigengene. Vertical dashed lines indicate the position of SNPs S5_88793314 (on the left) and AX-91658235 (on the right). The position of two transcription factors (a SBP gene, GRMZM2G111136, and a C2C2-CO-like transcription factor, GRMZM2G148772) representing promising candidate genes are indicated.